DUST DYNAMICS IN COMPRESSIBLE MAGNETOHYDRODYNAMIC TURBULENCE

Huirong Yan,[1] A. Lazarian,[1] and B. T. Draine[2]

ABSTRACT

We calculate the relative grain-grain motions arising from interstellar magnetohydrodynamic (MHD) turbulence. The MHD turbulence includes both fluid motions and magnetic fluctuations. While the fluid motions accelerate grains through hydrodrag, the electromagnetic fluctuations accelerate grains through resonant interactions. We consider both incompressive (Alfvén) and compressive (fast and slow) MHD modes and use descriptions of MHD turbulence obtained by Cho and Lazarian in 2002. Calculations of grain relative motion are made for realistic grain charging and interstellar turbulence that are consistent with the velocity dispersions observed in diffuse gas, including cutoff of the turbulence from various damping processes. We show that fast modes dominate grain acceleration and can drive grains to supersonic velocities. Grains are also scattered by gyroresonance interactions, but the scattering is less important than acceleration for grains moving with sub-Alfvénic velocities. Since the grains are preferentially accelerated with large pitch angles, the supersonic grains will be aligned with long axes perpendicular to the magnetic field. We compare grain velocities arising from MHD turbulence with those arising from photoelectric emission, radiation pressure, and H_2 thrust. We show that for typical interstellar conditions, turbulence should prevent these mechanisms from segregating small and large grains. Finally, gyroresonant acceleration is bound to preaccelerate grains that are further accelerated in shocks. Grain-grain collisions in the shock may then contribute to the overabundance of refractory elements in the composition of Galactic cosmic rays.

Subject headings: dust, extinction — ISM: kinematics and dynamics — ISM: magnetic fields — MHD — turbulence

Online material: color figure

1. INTRODUCTION

Dust is an important constituent of the interstellar medium (ISM). It interferes with observations in the optical range but provides insight into star formation activity through far-infrared radiation. It also enables molecular hydrogen formation and traces the magnetic field via emission and extinction polarization (see the reviews by Hildebrand et al. 2000; Lazarian 2000, 2003). The basic properties of dust (extinction, polarization, etc.) strongly depend on its size distribution. The latter evolves as the result of grain collisions, whose frequency and consequences depend on the grain relative velocities (see the discussions in Draine 1985; Lazarian & Yan 2002a, hereafter LY02; 2002b).

Grain-grain collisions can have various outcomes, e.g., coagulation, cratering, shattering, and vaporization. For collisions with $\delta v \leq 10^{-3}$ km s^{-1}, grains are likely to stick or coagulate, as the potential energy due to surface forces exceeds the initial center of mass kinetic energy. Coagulation is considered the mechanism to produce large grains in dark clouds (DCs) and accretion disks. Collisions with $\delta v \geq 20$ km s^{-1} have sufficient energy to vaporize at least the smaller of the colliding grains (Draine 1985). It is likely that some features of the grain distribution, e.g., the cutoff at large sizes (e.g., Kim et al. 1994), are the result of fragmentation (Biermann & Harwit 1980). Even low-velocity grain collisions may have dramatic consequences by triggering grain mantle explosion (Greenberg & Yencha 1973; Schutte & Greenberg 1991).

Various processes can affect the velocities of dust grains. Radiation, ambipolar diffusion, and gravitational sedimentation all can bring about a dispersion in grain velocities. It is widely believed that, except in special circumstances (e.g., near a luminous young star or in a shock wave), none of these processes can provide substantial random velocities so as to affect the interstellar grain population via collisions (Draine 1985), except for possibly enhancing the coagulation rate. Nevertheless, de Oliveira–Costa et al. (2002) speculated that starlight radiation could produce the segregation of different-sized grains that was invoked to explain the imperfect correlation of the microwave and 100 μm signals of the foreground emission (Mukherjee et al. 2001). If true, it has important implications for the cosmic microwave background foreground studies. However, the efficiency of this segregation depends on grain random velocities, which we study in this paper.

The ISM is magnetized and turbulent (see Arons & Max 1975; Scalo 1987; Lazarian 1999). Although turbulence has been invoked by a number of authors (see Kusaka et al. 1970; Völk et al. 1980; Draine 1985; Ossenkopf 1993; Weidenschilling & Ruzmaikina 1994) to provide substantial grain relative motions, the turbulence they discussed was not magnetized. Dust grains are charged, and their interactions with magnetized turbulence are very different from the hydrodynamic case. LY02 and Lazarian & Yan (2002b) applied the theory of Alfvénic turbulence (Goldreich & Sridhar 1995, hereafter GS95; see Cho et al. 2002a for a review) to grain acceleration and considered the motions that emerged as a result of incomplete coupling of grains and gas. Unlike the pure hydrodynamic case discussed by earlier authors, LY02 took into account that the motions of grains are restricted by magnetic fields in the direction perpendicular to the field lines, and also took into account the anisotropy of Alfvénic turbulence.

[1] Department of Astronomy, University of Wisconsin, 475 North Charter Street, Madison, WI 53706; yan@astro.wisc.edu, lazarian@astro.wisc.edu.
[2] Princeton University Observatory, Peyton Hall, Princeton, NJ 08544; draine@astro.princeton.edu.

While Alfvénic turbulence is the turbulence in an incompressible fluid, the ISM is highly compressible. Compressible MHD turbulence has been studied recently (see the review by Cho & Lazarian 2004 and references therein). In Yan & Lazarian (2003, hereafter YL03) we identified a new mechanism of grain acceleration, gyroresonance, which is based on the direct interaction of charged grains with MHD turbulence. YL03 provided a test calculation of grain acceleration in compressible MHD turbulence, by both hydrodrag and gyroresonance (see also the review by Lazarian & Yan 2004).

In what follows we describe grain acceleration by MHD turbulence in different phases of the ISM. Solving the Fokker-Planck equation including simultaneously the hydrodrag and gyroresonance would be a formidable task, which we do not attempt here. Instead, we try to simplify the problem by separating these two processes. For the random fluid drag, we use a simple scaling argument similar to the approach in Draine (1985) and LY02. While dealing with gyroresonance, we follow the approach adopted in YL03; i.e., we do not include the motion of ambient gas and assume that turbulence provides nothing but electromagnetic fluctuations. These approximations should yield correct answers when one of the mechanisms is dominant. When the accelerations arising from the two mechanisms are comparable, the situation is more complicated, as the gaseous friction that we use for gyroresonance calculations is, in general, affected by fluid motions. We do not develop an explicit theory for this case, but taking into account that it is the motions at the decoupling scale that accelerate grains via hydrodrag, we think it is reasonable to estimate the velocity gains from the simultaneous action of hydrodrag and gyroresonance by adding them in quadrature.

To describe the turbulence we use the statistics of Alfvén modes obtained in Cho et al. (2002b, hereafter CLV02) and of compressive modes obtained in Cho & Lazarian (2002, hereafter CL02; 2003a, hereafter CL03; 2003b).[3] We apply our results to different phases of the ISM, including the cold neutral medium (CNM), warm neutral medium (WNM), and warm ionized medium (WIM) and to molecular cloud (MC), and DC conditions, to estimate the implications for coagulation, shattering, and segregation of grains.

In what follows we introduce the statistical description of MHD turbulence and damping processes (§ 2), describe motions arising from hydrodrag (§ 3) and gyroresonance (§ 4), apply our results to various ISM phases (§ 5), discuss the astrophysical implications of our results (§ 6), and provide the summary in § 7.

2. MHD CASCADE AND ITS DAMPING

MHD perturbations can be decomposed into Alfvén, slow, and fast modes (see Alfvén & Fälthmmar 1963). Alfvénic turbulence is considered by many authors as the default model of interstellar magnetic turbulence. This is partially motivated by the fact that unlike compressive modes, the Alfvén modes are essentially free of damping in a fully ionized medium (see Ginzburg 1961; Kulsrud & Pearce 1969). Important questions arise. Can the MHD perturbations that characterize turbulence be separated into distinct modes? Can linear modes be used for this purpose? The separation into Alfvén and pseudo-Alfvén modes is the cornerstone of the GS95 model of turbulence.

This model and the legitimacy of the separation were tested successfully with numerical simulations (Cho & Vishniac 2000; Maron & Goldreich 2001; CLV02). Separation of MHD perturbations in compressible media into fast, slow, and Alfvén modes is discussed in GS95, Lithwick & Goldreich (2001), and CL02. The actual decomposition of MHD turbulence into Alfvén, slow, and fast modes was performed in CL02 and CL03, who also quantified the intensity of the interaction between different modes (see below).

Unlike hydrodynamic turbulence, Alfvénic turbulence is anisotropic, with eddies elongated along the magnetic field (see Montgomery & Matthaeus 1981; Shebalin et al. 1983; Higdon 1984; Zank & Matthaeus 1992). This happens because it is easier to mix the magnetic field lines perpendicular to the direction of the magnetic field rather than to bend them. The GS95 model describes *incompressible* Alfvénic turbulence, which formally means that the plasma $\beta \equiv P_{\mathrm{gas}}/P_{\mathrm{mag}}$, i.e., the ratio of gas pressure to magnetic pressure, is infinity. The turbulent velocity spectrum is easily obtained. Calculations in CLV02 prove that motions perpendicular to the magnetic field lines are essentially hydrodynamic. As a result, the energy transfer rate due to those motions is a constant $\dot{E}_k \sim v_k^2/\tau_k$, where τ_k is the energy eddy turnover time $\sim (v_k k_\perp)^{-1}$ and $k_\perp$ is the perpendicular component of the wavevector $\boldsymbol{k}$. The mixing motions couple to the wavelike motions parallel to magnetic field, giving a critical balance condition, i.e., $k_\perp v_k \sim k_\parallel V_A$, where $k_\parallel$ is the parallel component of the wavevector $\boldsymbol{k}$ and V_A is the Alfvén speed. From these arguments, the scale-dependent anisotropy $k_\parallel \propto k_\perp$ and a Kolmogorov-like spectrum for the perpendicular motions $v_k \propto k^{-1/3}$ can be obtained.

It was conjectured in Lithwick & Goldreich (2001) that the GS95 scaling should be approximately true for Alfvén and slow modes in moderately compressible plasma. For magnetically dominated (i.e., low β) plasma, CL02 showed that the coupling of Alfvén and compressive modes is weak and that the Alfvén and slow modes follow the GS95 spectrum. This is consistent with the analysis of H I velocity statistics (Lazarian & Pogosyan 2000; Stanimirovic & Lazarian 2001), as well as with electron density statistics (see Armstrong et al. 1995). Calculations in CL03 demonstrated that fast modes are marginally affected by Alfvén modes and follow an acoustic cascade in both high- and low-β media. In what follows we consider both Alfvén modes and compressive modes and use the description of those modes obtained in CL02 and CL03 to study dust acceleration by MHD turbulence.

The distribution of energy between compressive and incompressive modes depends, in general, on the driving of turbulence. CL02 and CL03 studied the generation of compressive perturbations using random incompressive driving, obtaining an expression that relates the energy in fast $\sim \delta V_f^2$ and Alfvén $\sim \delta V_A^2$ modes,

$$(\delta V_f / \delta V_A)^2 \sim \delta V_A \, V_A / (V_A^2 + C_s^2),$$

where C_s is the sound speed. This relation testifies that at large scales incompressive driving can transfer an appreciable part of energy into fast modes. However, at smaller scales the drain of energy from Alfvén to fast modes is marginal. Therefore, the cascades evolve without much cross talk. A more systematic study of different types of driving is required. In what follows we assume that equal amounts of energy are transferred into fast and Alfvén modes when driving is at large scales.
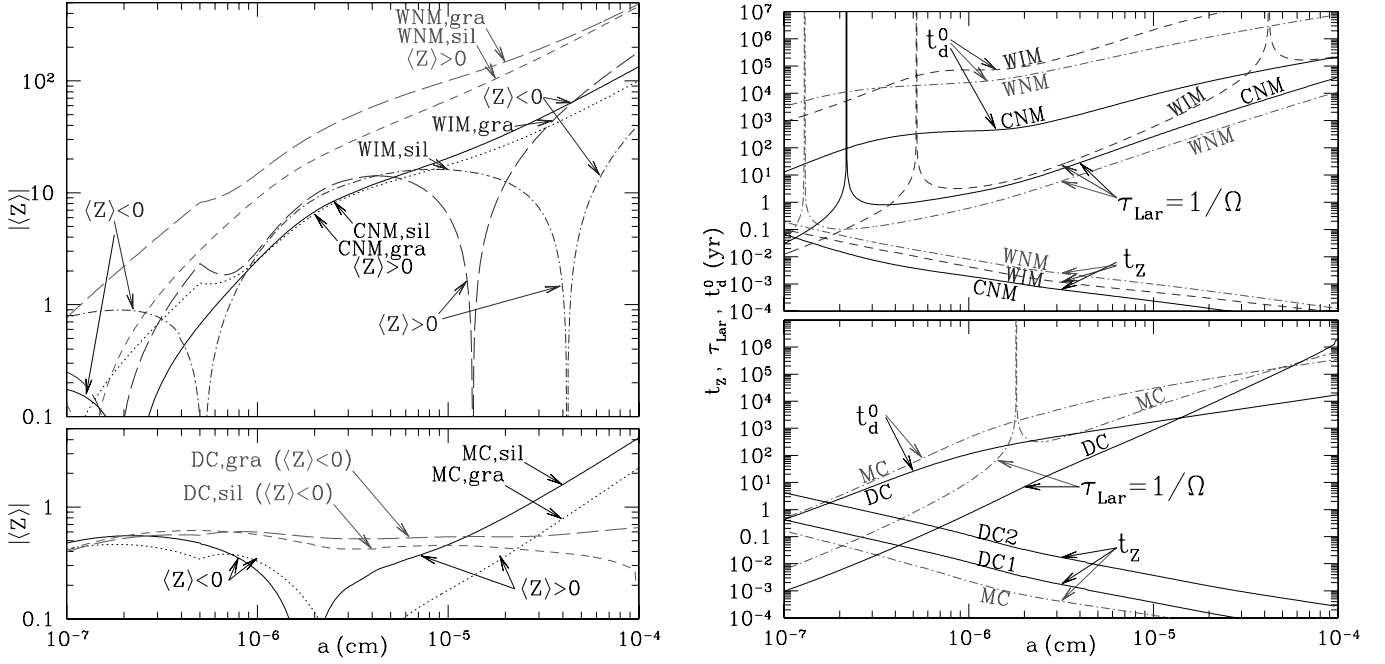
---

[3] The limitations on the applicability of such an approach are described in Yan & Lazarian (2003).

Fig. 1.—*Left*: $|\langle Z \rangle|$ as a function of grain radius for carbon and silicate grains in six different environments: CNM, WNM, WIM, MC, DC1, and DC2. The $|\langle Z \rangle|$ distribution is the same for DC1 and DC2, which are referred to as DC in the plot. *Right*: Gas-drag time t_d^0 for subsonic grains, the Larmor time $\tau_{\rm Lar}$, and the charge relaxation timescale t_Z, all as a function of grain size for silicate grains in the six different environments. [*See the electronic edition of the Journal for a color version of this figure.*]

We show that while simple scaling relations are sufficient for obtaining the velocities arising from hydrodrag, much more sophisticated tools are necessary for calculating gyroresonance (see Yan & Lazarian 2002, hereafter YL02; YL03). The corresponding statistics of turbulence is presented in Appendix B.

At small scales the turbulence spectrum is truncated by damping. Various processes can damp the MHD motions. In partially ionized plasma, the ion-neutral collisions are the dominant damping process. In fully ionized plasma, there are basically two kinds of damping: collisional and collisionless damping (see Appendix A for details). Their relative importance depends on the mean free path

$$l = v_{\rm th}\tau = \frac{6 \times 10^{11}(T/8000 \text{ K})^2 \text{ cm}^{-2}}{n}$$

in the ISM (Braginskii 1965). If the wavelength is larger than the mean free path, viscous damping dominates. If, on the other hand, the wavelength is smaller than the mean free path, the plasma is in the collisionless regime, and collisionless damping is dominant.

To obtain the truncation scale, the damping time should be compared with the cascading time. As we mentioned earlier, the Alfvénic turbulence cascades over one eddy turnover time $(k_\perp v_k)^{-1} \sim (k_\parallel V_{\rm A})^{-1}$. The cascade of the fast modes is a bit slower:

$$\tau_k = \omega/k^2 v_k^2 = (k/L)^{-1/2} V_f/V^2, \qquad (1)$$

where V_f is the phase velocity of fast waves and V is the turbulence velocity at the injection scale (CL02). If the damping is faster than the cascade, the turbulence is truncated. Otherwise, for the sake of simplicity, we ignore the damping and assume that the turbulence cascade is unaffected. According to CL02 the transfer of energy between Alfvén, slow, and fast modes of

MHD turbulence is suppressed. This allows us to consider different components of the MHD cascade independently.

3. GRAIN CHARGE

The net electrical charge on a grain is the result of competition between collisions with electrons, which add negative charge, and photoelectric emission and collisions with ions, which remove negative charge. We assume the grains to be spheres consisting of either "astronomical silicate" or graphite, with absorption cross sections calculated as described by Weingartner & Draine (2001a) and photoelectric yields (as a function of Z) as estimated by Weingartner & Draine (2001b).

The grain charge depends on the electron density n_e. While many previous studies have assumed cosmic-ray ionization rates $\zeta \approx 1 \times 10^{-17}$ s^{-1} (e.g., Ruffle et al. 1998), recent observational determinations (Black & van Dishoeck 1991; Lepp 1992; McCall et al. 2003) suggest $\zeta \approx (1-10) \times 10^{-16}$ s^{-1} in H I clouds. We adopt an electron density $n_e \approx 0.03$ cm^{-3} for CNM conditions, consistent with a detailed study of the ionization toward 23 Ori (Welty et al. 1999; Weingartner & Draine 2001c), corresponding to an H ionization rate $\zeta \approx 1.5 \times 10^{-16}$ s^{-1}.

For the outer regions of MCs we take $n_{\rm H} \approx 300$ cm^{-3} and $n_e/n_{\rm H} \approx 10^{-4}$, mainly because of photoionization of metals, where $G_{\rm UV} = 0.1$ is the UV intensity relative to the average interstellar radiation field. For DCs with $n_{\rm H} \approx 10^4$ cm^{-3}, we consider $G_{\rm UV}/n_e = 1$ cm^3, resulting in negatively charged grains.

Figure 1 (*left*) shows the mean grain charge $\langle Z \rangle$ for graphite and silicate grains in various phases of the ISM (see Table 1). The charge on a given grain fluctuates. Let f_Z be the probability of the grain being in charge state Z, and let r_Z be the probability per unit time of leaving charge state Z. The characteristic timescale for the grain charge to fluctuate is $t_Z \equiv \langle (Z - \langle Z \rangle)^2 \rangle / \sum_Z f_Z r_Z$. Figure 1 (*right*) compares the charge fluctuation time t_Z with the Larmor time (the Larmor period

TABLE 1
THE PARAMETERS OF IDEALIZED ISM PHASES AND RELEVANT DAMPING

Parameter	CNM	WNM	WIM	MC	DC1	DC2
T (K)	100	6000	8000	25	10	10
$n_{\rm H}$ (cm^{-3})	30	0.3	0.1	300	10^4	10^4
n_e (cm^{-3})	0.03	0.03	0.0991	0.03	0.01	0.001
$G_{\rm UV}$	1	1	1	0.1	0.01	0.001
B (μG)	6	5.8	3.35	11	80	80
L (pc)	0.64[a]	100	100	1	1	1
$V = V_{\rm A}$ (km s^{-1})	2[a]	20	20	1.2	1.5	1.5
Damping	Neutral-ion	Neutral-ion	Collisional	Neutral-ion	Ion-neutral decoupling	Ion-neutral decoupling
k_c (cm^{-1})	7×10^{-15}	4×10^{-17}	...	4.5×10^{-14}	5.3×10^{-15}	5.3×10^{-17}

NOTES.—Among these parameters, $n_{\rm H}$ is the number density of H, n_e is the number density of electrons, $G_{\rm UV}$ is the UV intensity scale factor, L is the injection scale of fast modes, and V is the injection velocity. The dominant damping mechanisms for fast modes are given with the corresponding damping timescale τ_c. CNM: cold neutral medium; WNM: warm neutral medium; WIM: warm ionized medium; MC: molecular cloud; DC: dark cloud.

[a] See the text for the explanation of smaller L and V for CNM.

divided by 2π), $\tau_{\rm Lar} \equiv 1/\Omega = m_{\rm gr}c/\langle Z \rangle eB$, and the gas drag timescale $t_{\rm drag}^0$ for subsonic motion. We see that, except for $a \lesssim 10^{-6}$ cm grains in DCs, the grain charge fluctuation time is much shorter than either of these dynamical times, so that these fluctuations can be ignored and the charge on a given grain can be assumed to be constant, equal to the time-averaged charge $\langle Z \rangle$.

4. GRAIN MOTIONS ARISING FROM HYDRODRAG

In hydrodynamic turbulence, the grain motions are caused by frictional interaction with the gas. On large scales grains are coupled with the ambient gas, and the fluctuating gas motions mostly cause an overall advection of the grains with the gas (Draine 1985). At small scales grains are decoupled. The largest velocity difference occurs on the largest scale at which grains are still decoupled. Thus, the characteristic velocity of a grain with respect to the gas corresponds to the velocity dispersion of the turbulence on the timescale t_d. In the MHD case, the charged grains are subject to electromagnetic forces. If $\tau_{\rm Lar} > t_d$, the grain does not feel the magnetic field. Otherwise, if $\tau_{\rm Lar} < t_d$, grain perpendicular motions are constrained by the magnetic field.

As Alfvénic turbulence is anisotropic, it is convenient to consider separately grain motions parallel and perpendicular to the magnetic field. The motions perpendicular to the magnetic field are influenced by Alfvén modes, while those parallel to the magnetic field are subjected to the magnetosonic modes. According to § 2, the perpendicular velocity field scales as $v_k \approx V(\tau_k/\tau_{\rm max})^{1/2}$, where $\tau_{\rm max} = L/V$ is the timescale of the injection.

If the Larmor time $\tau_{\rm Lar} < t_d$, grain perpendicular motions are constrained by the magnetic field. In this case, grains have a velocity dispersion determined by the turbulence eddy whose turnover period is $\sim\tau_{\rm Lar}$, while grains move with the magnetic field on longer timescales. Since the turbulence velocity grows with the eddy size, the largest velocity difference occurs on the largest scale at which grains are still decoupled. Thus, following the approach in Draine (1985), we can estimate the characteristic grain velocity relative to the fluid as the velocity of the eddy with a turnover time equal to $\tau_{\rm Lar}$,

$$v_\perp(a) = \frac{V^{3/2}}{L^{1/2}} (\rho_{\rm gr})^{1/2} \left(\frac{8\pi^2 c}{3qB} \right)^{1/2} a^{3/2}$$
$$= 0.9 \times 10^5 \text{ cm s}^{-1} \frac{(V_5 a_5)^{3/2}}{(Z L_{10} B_\mu)^{1/2}}, \quad (2)$$

in which $V_5 = V/10^5$ cm s^{-1}, $a_5 = a/10^{-5}$ cm, $Z = q/e$, $L_{10} = L/10$ pc, $B_\mu = B/1$ μG, and $\rho_{\rm gr}$ is the mass density of the grains. We adopt $\rho_{\rm gr} = 3.8$ g cm^{-3} for silicate grains and $\rho_{\rm gr} = 2$ g cm^{-3} for carbonaceous grains.

Grain motions parallel to the magnetic field are induced by the compressive component of the slow mode, with $v_\parallel \approx V \tau_k/\tau_{\rm max}$.[4] For grain motions parallel to the magnetic field, the Larmor precession is unimportant, and the gas-grain coupling takes place on the translational drag time t_d. The drag time due to collisions with atoms $t_d' = (a\rho_{\rm gr}/n_n)(\pi/8m_n k_{\rm B}T)^{1/2}$, where a is the grain size, m_n is the mass of the gas species, and T is the temperature, is essentially the time for collisions with a mass of gas equal to the mass of the grain. The ion-grain cross section due to long-range the Coulomb force is larger than the atom-grain cross section. For subsonic motions, the effective drag time $t_d^0 = t_d'/\alpha$, where (Draine & Salpeter 1979)

$$\alpha = \left\{ 1 + \frac{n_{\rm H}}{2n_n} \sum_i x_i \left(\frac{m_i}{m_n} \right)^{1/2} \sum_Z f_Z \left(\frac{Ze^2}{ak_{\rm B}T} \right)^2 \right.$$
$$\left. \times \ln \left[\frac{3(k_{\rm B}T)^{3/2}}{2e^3 |Z| (\pi x n_{\rm H})^{1/2}} \right] \right\}^{-1}, \quad (3)$$

where x_i is the abundance, relative to hydrogen, of ion i with mass m_i, $x = \sum_i x_i$, and f_Z is the probability of the grain being in charge state Z.

The characteristic velocity of grain motions along the magnetic field is approximately equal to the parallel turbulent velocity of eddies with turnover time equal to t_d:

$$v_\parallel(a) = \alpha^{-1} \frac{V^2}{L} \left(\frac{\rho_{\rm gr}}{4n_n} \right) \left(\frac{2\pi}{m_n k_{\rm B}T} \right)^{1/2} a$$
$$= \frac{(3.8 \times 10^5 \text{ cm s}^{-1}) \alpha^{-1} V_5^2 a_5}{n L_{10} T_{100}^{1/2}}, \quad (4)$$

where $T_{100} = T/100$ K. Equation (4) is valid for subsonic motion, $v < (k_{\rm B}T/m_n)^{1/2}$.

When the grain velocity v relative to the gas becomes supersonic (Purcell 1969), the gas drag time $t_d \approx t_d^0/[1 + (9\pi/128)v^2/C_s^2]^{1/2}$. When $\tau_{\rm Lar} > t_d$, grains are no longer tied to the magnetic field. Since, at a given scale, the largest

---
[4] We assume that turbulence is driven isotropically at the injection scale L.

velocity dispersion is perpendicular to the magnetic field direction, the velocity gradient over the grain mean free path is maximal in the direction perpendicular to the magnetic field direction. The corresponding scaling is analogous to the hydrodynamic case, which was discussed in Draine (1985):

$$
\begin{aligned}
v(a) &= \frac{V^{3/2}}{L^{1/2}} t_d^{1/2} \\
&= \alpha^{-1/2} \frac{V^{3/2}}{L^{1/2}} \left(\frac{\rho_{\rm gr}}{4n_n}\right)^{1/2} \left(\frac{2\pi}{m_n k_{\rm B} T}\right)^{1/4} a^{1/2}.
\end{aligned}
\tag{5}
$$

It is easy to see that the grain motions are modified when the damping timescale of the turbulence τ_c is longer than either t_d or $\tau_{\rm Lar}$. In this case, a grain samples only a part of the eddy before gaining the velocity of the ambient gas. In a turbulent medium, the shear rate dv/dl increases with the decrease of eddy size. Thus, for $\tau_c > \max\{t_d,\ \tau_{\rm Lar}\}$, these smallest available eddies are the most important for grain acceleration. Consider first the perpendicular motions. If v_c is the velocity of the critically damped eddy, the distance traveled by the grain is $\triangle l \sim v_c \min(t_d,\ \tau_{\rm Lar})$. The shear rate dv/dl perpendicular to the magnetic field is τ_k^{-1}. Thus, the grain experiences a velocity difference in the direction perpendicular to the magnetic field of

$$
v_\perp \sim \triangle l \frac{dv}{dl} \sim \frac{v_c}{\tau_c} \min(t_d,\ \tau_{\rm Lar}).
\tag{6}
$$

For the parallel motions, $\triangle l \sim v_c t_d$. From the critical balance in the GS95 model, $k_\parallel V_{\rm A} \sim k_\perp v_\perp = \tau_k^{-1}$, the largest shear rate along the magnetic field should be $dv/dl = v_c k_\parallel \sim v_c/(V_{\rm A} \tau_c)$. Therefore, in the parallel direction, the grain experiences a velocity difference $V_{\rm A}/v_c$ times smaller, i.e.,

$$
v_\parallel \sim \frac{v_c^2}{V_{\rm A}} \frac{t_d}{\tau_c}.
$$

The velocity dispersion induced by the compressional motion associated with the fast modes also causes motion relative to the ambient gas. The velocity fluctuation for fast modes scales as $v_k \propto k^{-1/4} \propto \omega^{-1/4}$, where ω is the frequency of the fast modes. From similar considerations, we know that grains get velocity dispersions during $\min(\tau_{\rm Lar},\ t_d)$, i.e., $v \simeq V[\min(\tau_{\rm Lar},\ t_d)/\tau_{\rm max}]^{1/4}$. Grains with $\min(\tau_{\rm Lar},\ t_d) < \tau_c$, have reduced velocities

$$
v \sim v_c \tau_{\rm Lar}/\tau_c \sim V(\tau_{\rm Lar}/\tau_{\rm max})^{1/4}(\tau_{\rm Lar}/\tau_c)^{3/4},
$$

where v_c is the velocity of turbulence at the damping scale. From the scaling, we see that the decoupling from fast modes always brings larger velocity dispersions to grains than Alfvén modes ($v_k \propto k^{-1/3}$), except for the situation in which Alfvén modes dominate MHD turbulence. The velocity fluctuations associated with fast modes are always in the direction perpendicular to $\boldsymbol{B}$ in low-β media (see Appendix D). Thus, the grain velocities are also perpendicular to $\boldsymbol{B}$. In high-β media, grains can have velocity dispersion in any direction, as the velocity dispersions of fast modes are longitudinal, i.e., along $\boldsymbol{k}$.

5. ACCELERATION OF GRAINS BY GYRORESONANCE

Gyroresonance acceleration of charged grains by a spectrum of MHD waves decomposed into incompressive Alfvén and compressive fast and slow modes (see CL02) was first described in YL02. The resonance occurs when $\omega - k_\parallel v \mu = n\Omega$ ($n = 0, \pm 1, \pm 2, \ldots$), where ω is the wave frequency, $k_\parallel$ is the parallel component of wavevector $\boldsymbol{k}$ along the magnetic field, v is the grain velocity, μ is the cosine of the grain pitch angle relative to the magnetic field, and Ω is the Larmor frequency of the grain. There are two main types of resonant interactions: gyroresonance acceleration and transit acceleration. Transit acceleration ($n = 0$) requires longitudinal motions and only operates with compressive modes. It happens when $k_\parallel v \mu = \omega$, which requires the particle speed to be super-Alfvénic, $v > V_f \geq V_{\rm A}$. Although this condition is partially relieved owing to resonance broadening (see Yan & Lazarian 2004), transit acceleration of low-speed grains is marginal because sub-Alfvénic particles can hardly catch up with the moving magnetic mirror.

How can we understand grain gyroresonance? Gyroresonance occurs when the Doppler-shifted frequency of the wave in the grain's guiding center rest frame $\omega_{\rm gc} = \omega - k_\parallel v \mu$ is a multiple of the grain gyrofrequency. For low-speed grains, we only need to consider the resonance at $n = 1$. The gyroresonance changes both the direction and absolute value of the grain's momentum (i.e., scatters and accelerates the grain). The efficiency of the two processes for charged grains can be described by the Fokker-Planck coefficients $D_{\mu\mu}$ and D_{pp}/p^2, where p is the grain momentum. The ratio of the two rates depends on the ratio of the grain velocity and the Alfvén speed and on the pitch angle, $p^2 D_{\mu\mu}/D_{pp} = [(v\zeta/V_{\rm A}) + \mu]^2$, where $\zeta = 1$ for Alfvén waves and $\zeta = k_\parallel/k$ for fast modes (see Appendix B). We see that the scattering is less efficient for sub-Alfvénic grains unless most grains move parallel to the magnetic field. We show below that as the result of acceleration, μ will tend to 0. Therefore, in the zeroth-order approximation, we ignore the effect of scattering and assume that the pitch angle cosine μ does not change while a grain is accelerated. In this case, the Fokker-Planck equation, which describes the diffusion of grains in momentum space, can be simplified (see Pryadko & Petrosian 1997):

$$
\frac{\partial f^\mu}{\partial t} + v\mu \frac{\partial f^\mu}{\partial z} = \frac{1}{p^2} \frac{\partial}{\partial p} p^2 D_{pp}(\mu) \frac{\partial f^\mu}{\partial p},
\tag{7}
$$

where f is the distribution function. Apart from acceleration, a grain is subjected to gaseous friction. Thus, we describe the stochastic acceleration by the Brownian motion equation:

$$
m\frac{dv}{dt} = -\frac{v}{S} + Y,
\tag{8}
$$

where m is the grain mass, Y is the stochastic acceleration force, and $S = t_d/m$ is the mobility coefficient.

If we multiply equation (8) by v and take the ensemble average, we obtain

$$
m\frac{d\langle v^2 \rangle}{dt} = -\frac{\langle v^2 \rangle}{S} + \langle \dot{\epsilon}^\mu \rangle.
\tag{9}
$$

The steady solution is achieved when the derivative on the left-hand side is zero. Following an approach similar to that in Melrose (1980), we can get from equation (7) the energy gain rate for the grain with pitch angle μ:

$$
\langle \dot{\epsilon}^\mu \rangle = \frac{1}{p^2} \frac{\partial}{\partial p} \left[v p^2 D_{pp}(\mu) \right].
\tag{10}
$$

The Fokker-Planck coefficient $D_{pp}(\mu)$ is calculated below.

YL03 employed quasi-linear theory (QLT) to obtain $D_{pp}(\mu)$ (see also YL02 and Appendix B):[5]

$$
\begin{aligned}
D_{pp}(\mu) = \frac{\pi \Omega^2 (1 - \mu^2) p^2 V_A^2}{2v^2} & \left(\int dk^3 \frac{\tau_k^{-1}}{\tau_k^{-2} + \left(\omega - k_\parallel v \mu - \Omega \right)^2} \right. \\
& \times \left\{ J_2^2 \left(\frac{k_\perp v_\perp}{\Omega} \right) [K_{\mathcal{R}\mathcal{R}}(\boldsymbol{k}) + K_{\mathcal{L}\mathcal{L}}(\boldsymbol{k})] \right. \\
& + J_0^2 \left(\frac{k_\perp v_\perp}{\Omega} \right) [K_{\mathcal{R}\mathcal{R}}(\boldsymbol{k}) + K_{\mathcal{L}\mathcal{L}}(\boldsymbol{k})] \\
& - 2 J_2 \left(\frac{k_\perp v_\perp}{\Omega} \right) J_0 \left(\frac{k_\perp v_\perp}{\Omega} \right) \\
& \left. \left. \times \left[e^{i2\phi} K_{\mathcal{R}\mathcal{L}}(\boldsymbol{k}) + e^{-i2\phi} K_{\mathcal{L}\mathcal{R}}(\boldsymbol{k}) \right] \right\} \right).
\end{aligned} \tag{11}
$$

However, we should not integrate over all k, because the contribution from large scales is spurious (see discussion in YL02). This contribution stems from the fact that in QLT, an unperturbed grain orbit is assumed, which results in nonconservation of the adiabatic invariant $\xi = m v_\perp^2 / 2 B_0$. Noting that the adiabatic invariant is conserved when the electromagnetic field varies on a timescale longer than Ω^{-1}, we truncate our integral range, namely, integrate from k_{res} instead of the injection scale L^{-1}. For Alfvénic turbulence $\omega = |k_\parallel| V_A$, the resonant scale corresponds to $|k_{\parallel,\mathrm{res}}| = \Omega / |V_A - v\mu|$. For fast modes, the resonant scale is $k_{\mathrm{res}} = \Omega / |V_f - v\mu \cos\theta|$, where $\cos\theta = k_\parallel / k$. The upper limit of the integral k_c is set by the dissipation of the MHD turbulence, which varies with the medium.

Integrating from k_{res} to k_c, we obtain from equations (11) and (10) the energy gain rate $\dot{\epsilon}$ as a function of v and μ. Then, with $\dot{\epsilon}$ known, we estimate the grain acceleration. Solving equation (9) iteratively, we obtain the grain velocity as a function of time. We check that the grain velocities converge to a constant value after the drag time. As $\dot{\epsilon}$ increases with pitch angle, grains gain the maximum velocities perpendicular to the magnetic field, and therefore the averaged μ decreases. This is understandable, since the electric field, which accelerates the grain, is in the direction perpendicular to the magnetic field.

6. GRAIN MOTIONS IN THE ISM

Here we apply our results to various idealized phases of the ISM. First, consider a typical CNM, $T = 100$ K, $n_{\mathrm{H}} = 30$ cm^{-3}, $n_e = 0.045$ cm^{-3}, and $B = 6$ μG, with a corresponding $v_A = 2$ km s^{-1} and $\beta \sim 0.4$. Our treatment of MHD turbulence requires that fluid velocities be smaller than the Alfvén speed.[6] Therefore, we assume that the injection of energy happens at an effective injection scale L at which equipartition between magnetic and kinetic energies occurs, i.e., $V = V_A$. This effective injection scale can be different from the actual scale at which energy is injected. For instance, if we assume that the velocity dispersion at the scale $l = 10$ pc is 5 km s^{-1}, this means that turbulence in the CNM is super-Alfvénic at this scale. The turbulence then follows a hydrodynamic cascade down to a scale $L \approx 0.64$ pc at which the turbulent velocity becomes equal to $V_A = 2$ km s^{-1}; we identify this as the effective "injection scale" L[7] with injection velocity

$V = V_A = 2$ km s^{-1}. Alternatively, it is possible that the turbulence at large scales proceeds in tenuous warm media with an Alfvén speed larger than or equal to 5 km s^{-1}. Nevertheless, the statistics of fast modes will not be changed in the CNM.

In partially ionized media, the damping is dominated by the viscosity arising from neutrals. The turbulence is assumed damped[8] when its cascading timescale $\tau_k = t_{\mathrm{damp}}$; this defines the cutoff scale $k_{\parallel,c} = 4 \times 10^{-16}$ cm^{-1} for Alfvén modes and $k_c = 7 \times 10^{-15}$ cm^{-1} for fast modes (see Appendix A). Assuming that the grain velocities are smaller than the phase speed of the fast modes, we find that the prerequisite for gyroresonance $k_c > k_{\mathrm{res}}$ is the same as $\tau_{\mathrm{Lar}} > \tau_c$, the condition for effective hydrodrag (see Fig. 1). For a silicate grain, the critical grain size $a_c \approx 4 \times 10^{-6}$ cm for fast modes and $\approx 10^{-5}$ cm for Alfvén modes. Grains smaller than the critical size are not effectively accelerated by the corresponding turbulent mode.

The CNM is a low-β medium, so the correlation tensors for the low-β case are applied. As has been discussed in YL02, the interactions with Alfvén modes are less efficient than those with fast modes because of the anisotropy of Alfvén modes. Thus, we consider only fast modes for later calculations. The gyroresonance with fast modes in the CNM can accelerate grains to supersonic velocities, and $\dot{\epsilon}^\mu$ increases with pitch angle. If we average $\dot{\epsilon}$ over μ, we get mean velocities that are smaller than the maximum values by less than 20%. In Figure 2 we plot the velocity of grains with pitch angle equal to 90° as a function of grain size, since all the mechanisms preferentially accelerate grains in this direction.

For the WNM, $T = 6000$ K, $n_{\mathrm{H}} = 0.3$ cm^{-3}, $n_e = 0.03$ cm^{-3}, and $B = 5.8$ μG. We assume the velocity dispersion $V = V_A = 20$ km s^{-1} at the injection scale $L = 100$ pc. Turbulence is mainly subjected to neutral-ion damping. The fast modes are cut off at $k_c = 4 \times 10^{-17}$ cm^{-1} (see Appendix A). Comparing k_c with k_{res}, we find $a_c \approx 2 \times 10^{-5}$ cm for silicate grains. The WNM has $\beta \approx 0.25$, so we use the tensor given in equation (B4) for fast modes. Integrating from k_{res} to k_c and solving equation (9), we obtain the grain velocities. The maximum values are shown in Figure 3. We see that large grains can be accelerated to supersonic speeds.[9] The fact that these grains approach the Alfvén speed makes our approximation that acceleration dominates scattering less accurate, but the result is correct within a factor of unity. Smaller grains are accelerated only by the hydrodrag, which is far less effective.

The WIM has $T = 8000$ K, $n_e = 0.1$ cm^{-3}, and $B = 3.35$ μG, with a corresponding $\beta \sim 0.33$. The injection scale and speed are the same as in the WNM. The WIM is fully ionized and in the low-β regime. Fast modes, in this case, are mainly affected by collisional damping. This damping increases with θ[10] and does not exist for parallel modes (see Appendix A). Thus, there are always modes interacting with grains, although the energy available is less at smaller scales. Following the same routine as above, we get the grain velocities. We see from Figure 4 the nonmonotonic variation of grain velocity with the size. This arises from the fact that the charging for grains in the WIM has a complex dependence on grain size (see also Fig. 1, *left*).

---

[5] Usually the real part is taken of the integral. However, we show in Appendix B that the integrand is real.

[6] Otherwise, the magnetic field is not dynamically important. Turbulence is essentially hydrodynamic. See the following discussions.

[7] This picture is not self-consistent, as we expect to have turbulent generation of the magnetic field, which will bring kinetic and magnetic energy to equipartition at the injection scale (see the arguments in Cho et al. 2002a), but the idea of super-Alfvénic turbulence percolates in the literature (Boldyrev et al. 2002).

[8] Thus, we ignore the effect of slowly evolving magnetic structures associated with the recently reported new regime of turbulence below the viscous damping cutoff (Cho et al. 2002c; Lazarian et al. 2004).

[9] Unlike hydrodrag, gyroresonance can potentially accelerate grains to velocities much higher than the velocity of turbulent motions. For typical ISM conditions, however, this does not happen.

[10] This θ-dependence makes the treatment of damping more complicated if taking into account field line wandering (see Yan & Lazarian 2004).
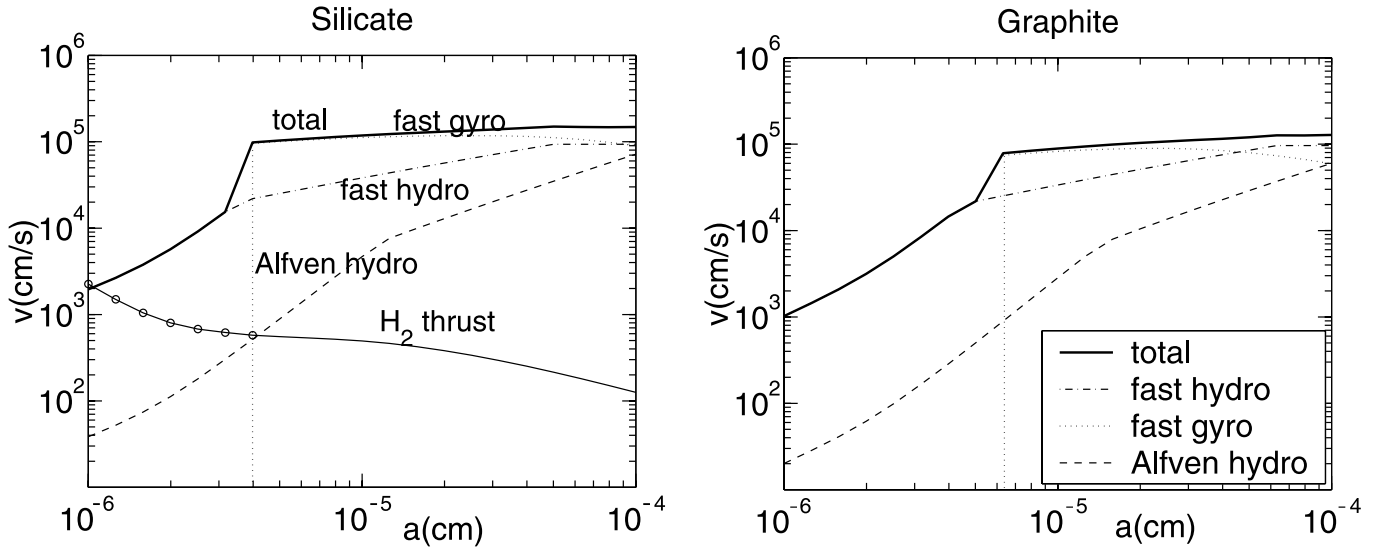
Fig. 2.—Relative velocities as a function of radii (*thick solid lines*) in CNM, for silicate grains (*left*) and graphite grains (*right*). The dotted lines represent the gyroresonance with fast modes. Gyroresonance works only for large grains because of the cutoff by viscous damping. The cutoff scales for fast and Alfvén modes are different because of their different scalings and the anisotropy of Alfvén modes. The dashed lines are the result with hydrodrag by Alfvén modes (see LY02), and the dash-dotted lines represent hydrodrag by fast modes. Contributions from different mechanisms are approximately additive in quadrature, i.e., $v_{\rm tot}^2 = \Sigma_i v_i^2$. The grain velocity driven by H₂ formation (*thin solid line*) is plotted to illustrate the issue of grain segregation in the CNM (see text). The part marked with open circles is nonphysical because thermal flipping is not taken into account.

MC gas has $T = 25$ K and $n_{\rm H} = 300$ cm^{-3}, and we adopt a magnetic field strength of $B = 11$ μG as suggested by observations (Crutcher 1999), corresponding to an Alfvén speed $V_A = 1.2$ km s^{-1}. The injection scale is taken to be $L = 1$ pc, and the injection velocity is $V = V_A$. The damping scale (see Appendix A) of the turbulence is $k_c = 4.5 \times 10^{-14}$ cm^{-1}, corresponding to resonant scales of silicate grains with $a = 8 \times 10^{-7}$ cm. By following the same procedure, we obtain the grain velocity distribution as shown in Figure 5.

We consider a typical DC with $T = 10$ K, $n_{\rm H} = 10^4$ cm^{-3}, and $B \sim 80$ μG, corresponding to $V_A = 1.5$ km s^{-1}. The injection scale $L = 1$ pc, and the velocity $V = V_A$. The ionization in a DC is so low that the fluid becomes decoupled in the middle of the cascade, where the ion-neutral collision rate t_{ni}^{-1} per neutral is equal to the turbulence decay rate τ_k^{-1}. Below this decoupling scale, neutrals will not follow ions and magnetic fields, and the turbulence becomes hydrodynamic. In view of

the uncertainty of the cosmic-ray ionization rate, we adopt two models, DC1 and DC2, with electron densities $n_e = 0.01$ cm^{-3} and $n_e = 0.001$ cm^{-3}. The grain charge distribution is the same for both DC1 and DC2, because we assume the same $G_{\rm UV}/n_e$. The main difference is the decoupling scale of the MHD cascade. Combining equations (1) and (A2), we can obtain the decoupling scales $k_c = 5.3 \times 10^{-15}$ cm^{-1} for DC1 and $k_c = 5.3 \times 10^{-17}$ cm^{-1} for DC2, corresponding to silicate grain size $a_c \approx 3 \times 10^{-6}$ cm for DC1 and $a_c \approx 2 \times 10^{-5}$ cm for DC2. By following the same procedure, we obtain the grain velocity distribution as shown in Figures 6 and 7.

It is shown in Figures 5–7 that the acceleration by gyroresonance in both MCs and DCs is not as effective as in the lower density media, for two reasons. First, the low levels of UV and low temperatures result in a reduced grain charge (see Fig. 1, *left*). Second, because of the increased density, the drag time t_d is reduced. The grain velocities in CNM found here are smaller
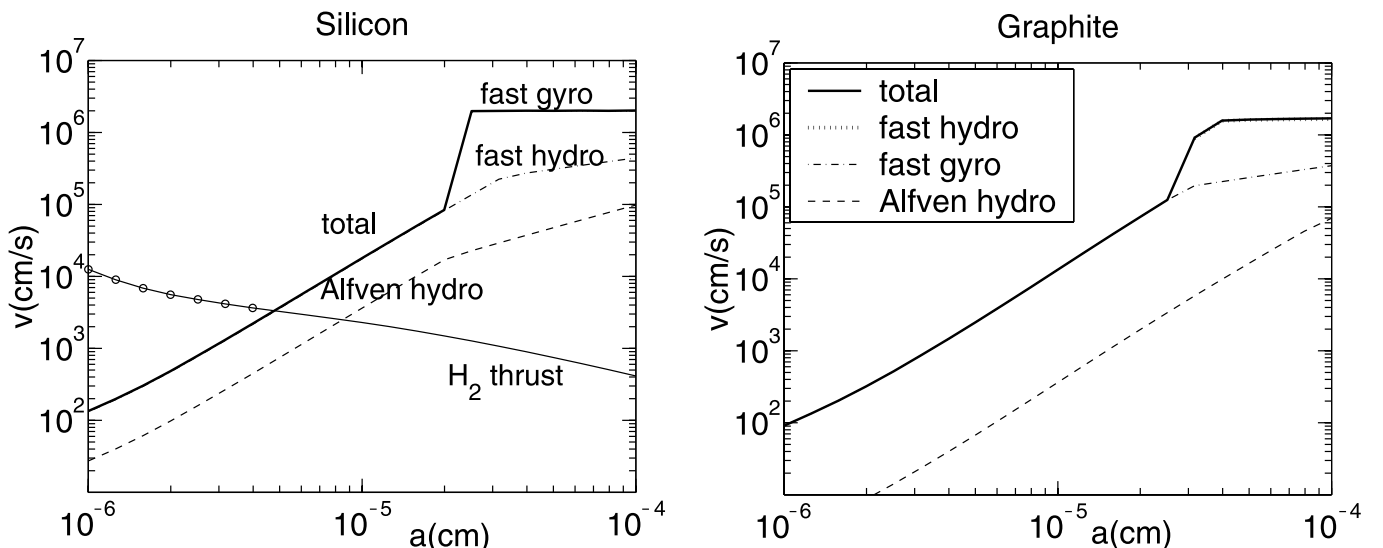
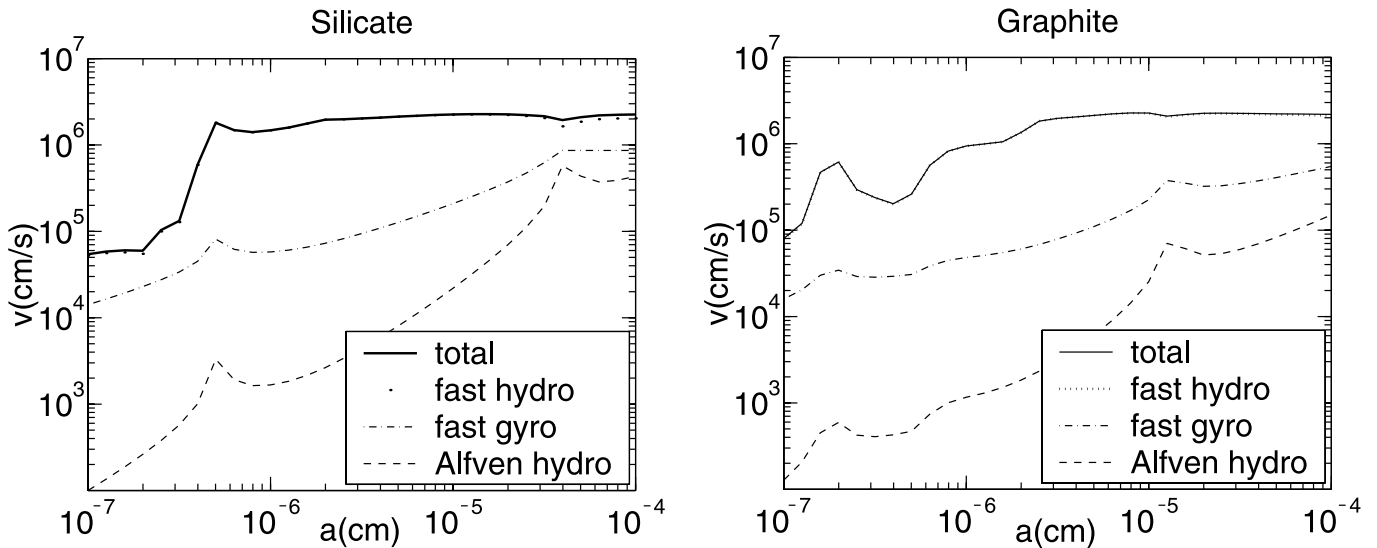Fig. 3.—Same as Fig. 2, but in the WNM.

Fig. 4.—Same as Fig. 2, but in the WIM. The oscillations in these curves are due to the variation in charging of grains.

than in an earlier calculation (see YL03) because we adopt smaller values for the magnetic field B and injection velocity V.

It should be noted that the strength of magnetic fields in the ISM is still somewhat uncertain and may vary from place to place. We adopted a particular set of values in the above calculations. How would the results vary as the magnetic field strength varies? First of all, we know that the critical condition for acceleration is $k_{res} > k_d$: grains with $k_{res} < k_d$ cannot be accelerated. Thus, the cutoff grain radius a_c varies with the medium, $a_c \approx [3q(a_c)\tau_c B/4\pi\rho]^{1/3}$; grains with $a < a_c$ are not subject to gyroresonant acceleration.

The magnitude of the velocity is a complex function of the magnetic field. For illustration, in Figure 8 we show the grain velocities calculated for magnetic fields a factor of 3 stronger or weaker than the values in Table 1 for the CNM and DC1 environment. Since the hydrodrag by fast modes decreases with the magnetic field, the relative importance of gyroresonance and hydrodrag depends on the magnitude of the magnetic field. In magnetically dominant regions, gyroresonance is dominant. In weakly magnetized regions, the frictional drag provides the

highest acceleration rate. The injection scale is another uncertain parameter, but the grain velocity is not as sensitive to it, provided that the injection scale is much larger than the damping scale.

7. DISCUSSION

7.1. Shattering and Coagulation

With the grain relative velocities known, we can make predictions for grain shattering and coagulation. For shattering, we adopt the Jones et al. (1996) results, namely, for equal-sized particles the shattering threshold is 2.7 km s^{-1} for silicate grains and 1.2 km s^{-1} for carbonaceous grains. The critical sticking velocity given by Chokshi et al. (1993; see also Dominik & Tielens 1997),[11]

$$v_{cr} = 2.14 F_{stick} \left[\frac{a_1^3 + a_2^3}{(a_1 + a_2)^3} \right]^{1/2} \frac{\gamma^{5/6}}{E^{1/3} R^{5/6} \rho^{1/2}},$$

[11] Note an error in the exponent of Young's modulus in eq. (10) of Dominik & Tielens (1997).
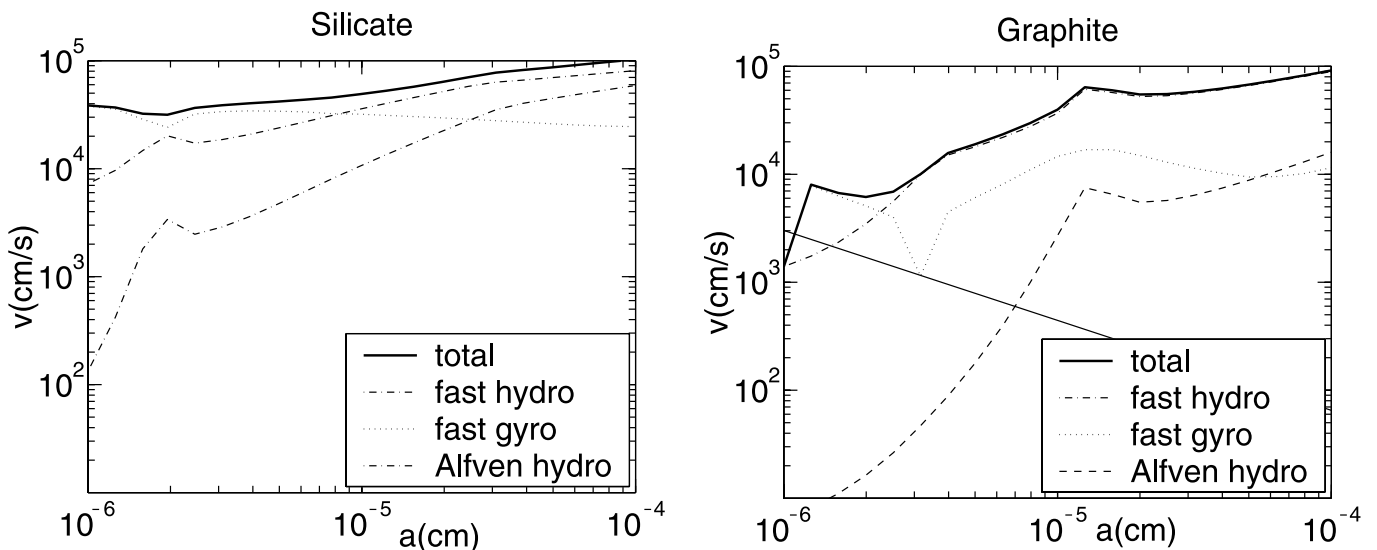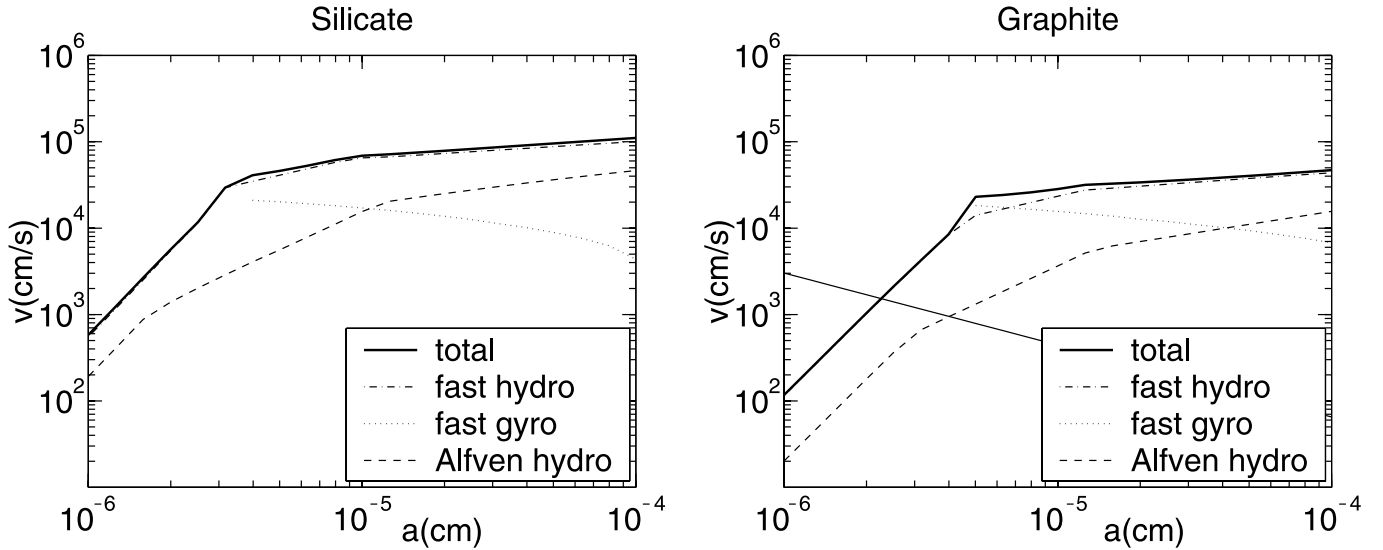

Fig. 5.—Same as Fig. 4, but in an MC.

Silicate

Graphite

Fig. 6.—Same as Fig. 2, but in a DC1.

is the maximum relative velocity for coagulation of equal-size spherical grains, where γ is the surface energy per unit area, $R = a_1 a_2 / (a_1 + a_2)$ is the reduced radius of the grains, E is related to Poisson's ratio ν_i and Young's modulus E_i by $1/E = [(1 - \nu_1)^2 / E_1 + (1 - \nu_2)^2 / E_2]$, and we have introduced a factor $F_{\text{stick}} \approx 10$, since the experimental work by Blum (2000) shows that the critical velocity is an order of magnitude higher than the theoretical estimate of Chokshi et al. We use γ, E, and ν for SiO_2 and graphite from Table 1 of Dominik & Tielens (1997) and consider collisions between equal-size grains ($a_1 \approx a_2$). Comparing these critical velocities with the velocity curve we obtained for various media, we can get the corresponding critical size for each of them (see Table 2).

7.2. *Correlation between Turbulence and Grain Sizes*

The grain velocities are strongly dependent on the maximal velocity of turbulence V at the injection scale, which is highly uncertain. The critical coagulation and shattering sizes thus also depend on the amplitude of the turbulence. Variations in the level of turbulence could lead to regional differences in the grain-size distribution.
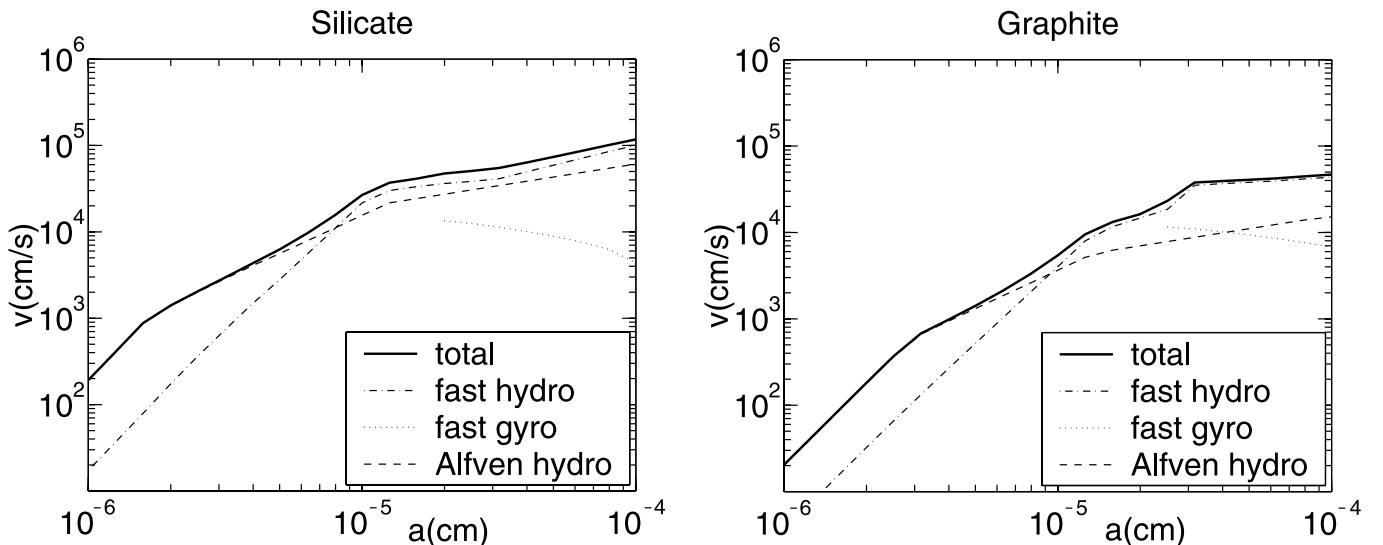
7.3. *Elements in Cosmic Rays*

It has been shown that the composition of Galactic cosmic rays appears to be correlated with elemental volatility (Ellison et al. 1997). The more refractory elements are systematically overabundant relative to the more volatile ones. This suggests that the material locked in grains must be accelerated more efficiently than gas-phase ions (Epstein 1980; Ellison et al. 1997). The stochastic acceleration of grains, in this case, can act as a preacceleration mechanism. The ions released from the grains in the shock by sputtering or in grain-grain collisions can then be further accelerated in the shock, which explains the overabundance of refractory elements in Galactic cosmic rays.

7.4. *Heavy-Element Depletion and Grain Alignment*

Our results indicate that grains can become supersonic through interaction with fast modes. Grains moving with velocities larger than those of heavy ions could sweep up heavy elements, which may be advantageous from the point of explaining observations (Wakker & Mathis 2000). Our calculations show that while such velocities are readily achievable,

Silicate
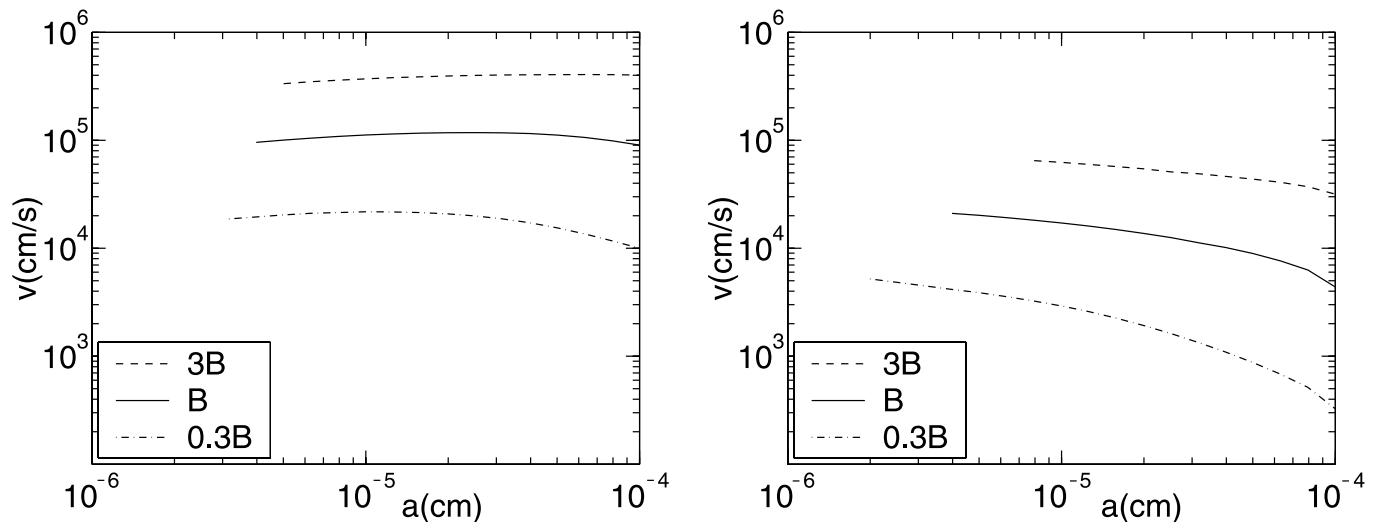
Graphite

Fig. 7.—Same as Fig. 2, but in a DC2.

FIG. 8.—Relative velocities gained from gyroresonance as a function of radii for different magnetic field strengths, in CNM (*left*) and a DC1 (*right*). Solid lines show the results for typical values of the magnetic field. Dashed lines refer to the results with a magnetic field 3 times stronger. Dash-dotted lines represent the cases with a magnetic field 3 times weaker.

the sign of charging may present a problem for such "vacuum cleaning" of the ISM. For instance, silicate grains in an MC can be accelerated to $\gtrsim 4 \times 10^4$ cm s^{-1}, which is larger than the thermal speed of heavy ions. Therefore, the capture rate for ions by positively charged grains ($\lesssim 2 \times 10^{-6}$ cm) would be increased. Grains smaller than 2×10^{-6} cm would be negatively charged in the MC. For such grains the cross section for Coulomb capture of ions would decrease. If such small grains retain captured ions, this would result in a decrease of the rate of depletion of metals on grains. The actual rates of depletion on fast-moving grains are important and will be identified elsewhere for particular phases of the ISM.

Grains moving supersonically can be aligned mechanically (see a review by Lazarian 2003 and references therein). As pointed out earlier, the scattering is not efficient for slowly moving grains, so we can ignore the effect of scattering on the pitch angle. Since the acceleration of grains increases with the pitch angle of the grain (see eqs. [10] and [11]), supersonic grains will tend to have large pitch angles. As first discussed by Gold (1952), gas drag acting on these grains will tend to cause them to spin with angular momenta perpendicular to their motion and therefore parallel to the magnetic field direction. Dissipational processes will tend to orient the spinning grains with their long axes perpendicular to their angular momentum, resulting in grain alignment with long axes perpendicular to the magnetic direction.

7.5. *Grain Segregation and Turbulent Mixing*

Our results are also relevant to grain segregation. Grains are the major carrier of heavy elements in the ISM. The issue of

grain segregation may have significant influence on the ISM metallicity. Subjected to external forcing (WD01; Ciolek & Mouschovias 1996), grains gain size-dependent velocities with respect to gas. WD01 considered the forces on dust grains exposed to anisotropic interstellar radiation fields, including photoelectric emission, photodesorption, and radiation pressure, and calculated the drift velocity for grains of different sizes. The velocities they got for silicate grains in the CNM range from 0.1 to 10^3 cm s^{-1}. Grains can move along magnetic field lines because of uncompensated forces, e.g., because of active sites of H_2 formation (see Purcell 1979; Lazarian & Yan 2002b).[12] Figure 2 (*left*) shows that turbulence produces larger velocity dispersions.[13] Those velocities are preferentially perpendicular to the magnetic field, but in many cases the dispersion of velocities parallel to the magnetic field is comparable to the regular velocities above. This dispersion stems both from the fact that the transpositions of matter by fast modes are not exactly perpendicular to the magnetic field (see plot in Lazarian & Yan 2002b) and from the randomization of the directions of grain velocities by magnetized turbulence (YL03).

More important is that if reconnection in the turbulent medium is fast (see Lazarian & Vishniac 1999; Lazarian et al. 2004), the mixing of grains over large scales is provided by turbulent diffusivity $\sim VL/4$. Usually, it has been assumed that magnetic fields strongly suppressed the diffusion of charged

[12] These forces would be mitigated in MCs, which would induce inflow of dust into the MC. The latter would affect the metallicity of newborn stars.

[13] Our calculations show that for the chosen set of parameters, the effects of systematic thrust are also limited (see LY02; Lazarian & Yan 2002b).

TABLE 2
SIZE RANGES FOR SHATTERING AND COAGULATION IN DIFFERENT MEDIA

	CNM		WNM		WIM		DC1		DC2	
PROCESS	Silicate	Carbon	Silicate	Carbon	Silicate	Carbon	Silicate	Carbon	Silicate	Carbon
Shattering	...	...	>0.2	>0.2	>0.003	>0.001	...	...	...	...
Coagulation	<0.01	<0.02	<0.02	<0.04	...	...	≲0.01	<0.02	<0.02	<0.04

NOTES.—Size ranges are in microns. CNM: cold neutral medium; WNM: warm neutral medium; WIM: warm ionized medium; MC: molecular cloud; DC: dark cloud.

species perpendicular to their directions. However, this assumption is questionable if we note that motions perpendicular to the local magnetic field are hydrodynamic to high order, as suggested by Cho et al. (2002a). Recent work by Cho et al. (2003) found that the diffusion processes in MHD turbulence are almost as effective as in the hydrodynamic case if the mean magnetic field is weak or moderately strong (i.e., B less than or equal to the equipartition value), which would imply that grains can be mixed by the MHD turbulence. Lazarian & Yan (2004) therefore concluded that the segregation of very small and large grains speculated about in de Oliveira–Costa et al. (2002) is unlikely to happen for typical interstellar conditions.

8. SUMMARY

We have calculated the relative motions of dust grains in a magnetized turbulent fluid. It has been known for decades that turbulence can give rise to significant grain-grain velocities. However, earlier treatments disregarded the magnetic field and used Kolmogorov turbulence. Magnetohydrodynamic (MHD) turbulence includes both fluid motions and magnetic fluctuations. While the fluid motions bring about decoupled motions to grains, the electromagnetic fluctuations can accelerate grains through resonant interactions.

Calculations of grain relative motion are made for different phases of the ISM with realistic grain charging and with turbulence that is consistent with the velocity dispersions observed in interstellar gas. We account for the cutoff of the turbulence from various damping processes. We show that fast modes dominate grain acceleration and can drive grains to supersonic velocities. Grains are also scattered by gyroresonance interactions. The scattering rate is less efficient than acceleration for grains moving with sub-Alfvénic velocities. Since the grains are preferentially accelerated with large pitch angles, the supersonic grains tend to be aligned with their long axes perpendicular to the magnetic field.

Gyroresonant acceleration is bound to preaccelerate grains that will then be further accelerated by shocks. Grain-grain collisions and sputtering in the shocks will inject suprathermal ions that can then undergo further acceleration in the shock, potentially accounting for the observed excess of refractory elements in the composition of Galactic cosmic rays (e.g., Epstein 1980; Ellison et al. 1997).

APPENDIX A

DAMPING OF MHD WAVES

Below we summarize the damping processes that we consider in the paper.

A1. NEUTRAL-ION DAMPING

In a partially ionized medium, a combination of neutral viscosity and ion-neutral collisional coupling provides damping (see LY02). If the mean free path for a neutral l_n in a partially ionized gas with density $n_{tot} = n_n + n_i$ is much less than the size of the eddies under consideration, i.e., $l_n k \ll 1$, the damping time

$$t_{damp} \sim \nu_n^{-1} k^{-2} \sim \frac{n_{tot}}{n_n} (l_n v_n)^{-1} k^{-2}, \tag{A1}$$

where ν_n is the effective viscosity produced by neutrals,[14] v_n is the thermal velocity of the neutrals, and the mean free path of a neutral l_n is influenced by collisions with both neutrals and ions. The rate at which neutrals collide with ions is proportional to the density of ions, while the rate at which neutrals collide with other neutrals is proportional to the density of neutrals. The momentum transfer rate coefficient for neutral-neutral collisions is $\sim 1.7 \times 10^{-10} (T/1 \text{ K})^{0.3}$ cm^3 s^{-1} (Spitzer 1978), while for neutral-ion collisions it is $\sim \langle v_r \sigma_{in} \rangle \approx 1.9 \times 10^{-9}$ cm^3 s^{-1} (Draine et al. 1983). Thus, collisions with other neutrals dominate for $n_i/n_n \lesssim 0.09 T^{0.3}$.

A2. EFFECTS OF CHARGED GRAINS

Magnetic perturbations can get decoupled from the fluid motions because neutrals are imperfectly coupled to the ions in a partially ionized medium.[15] The coupling between ions and neutrals is determined by the ion-neutral collision rate:

$$t_{ni}^{-1} = \frac{m_i}{m_n + m_i} n_i \langle v_r \sigma_{in} \rangle, \tag{A2}$$

where v_r is the ion-neutral relative velocity, σ_{in} is the ion-neutral collisional cross section, m_i and m_n are the typical ion and neutral masses, and n_i is the ion number density. When the collisional time t_{ni} is equal to the wave period, neutrals are decoupled from the magnetic field, and the turbulence becomes hydrodynamic. In MCs, grains can take a substantial portion of the total charge. The

---

[14] The viscosity due to ion-ion collisions is typically small, as ion motions are constrained by the magnetic field.

[15] We do not discuss here the viscosity-damped regime of MHD turbulence that takes place in the partially ionized gas below the scale at which viscosity damps kinetic motions associated with the magnetic field (see the theory on this regime in Lazarian et al. 2004).

contribution of charged grains to coupling neutrals with magnetic fields depends on the grain-size spectrum. The ratio of the ion-neutral collision rate to the grain-neutral collision rate is

$$\frac{t_{ni}^{-1}}{\langle n_g \sigma_g \rangle v_n} \simeq \begin{cases} 0.25 n_4^{-1/2}, & \text{MRN}, \\ 3.3 n_4^{-1/2}, & \text{MW} \end{cases} \tag{A3}$$

(Nishi et al. 1991; Elmegreen & Fiebig 1993), where MRN refers to the grain-size distribution proposed by Mathis et al. (1977) and MW stands for the distribution suggested by Mathis & Whiffen (1989). From this expression we can see that ions are always the dominant contribution for the coupling in MCs. In DCs the situation will depend on the grain-size distribution. A DC is a denser region in which observations favor MW distribution (Elmegreen & Fiebig 1993). Thus, presumably, the contribution from grains in a DC is also subdominant, and we neglect it in the main text.

A3. COLLISIONLESS DAMPING

The nature of collisionless damping is closely related to the radiation of charged particles in the magnetic field. Since the charged particles can emit plasma waves through acceleration (cyclotron radiation) and the Cerenkov effect, they also absorb radiation under the same conditions (Ginzburg 1961). The damping rate $\gamma_d = \tau_d^{-1}$ of the fast modes of frequency ω for $\beta \ll 1$ and $\theta \sim 1$ (Ginzburg 1961) is

$$\Gamma_d = \frac{\sqrt{\pi\beta}}{4} \omega \frac{\sin^2\theta}{\cos\theta} \left[\sqrt{\frac{m_e}{m_H}} \exp\left(-\frac{m_e}{m_H \beta \cos^2\theta} \right) + 5 \exp\left(-\frac{1}{\beta \cos^2\theta} \right) \right], \tag{A4}$$

where m_e is the electron mass. The exact expression for the damping of fast waves at small θ was obtained by Stepanov (1958):[16]

$$\Gamma_d = \frac{\sqrt{\pi\beta}}{4} \omega \theta^2 \left(1 + \frac{\theta^2}{\sqrt{\theta^4 + 4\Omega_i^2/\omega^2}} \right) \sqrt{\frac{m_e}{m_H}} \exp\left(-\frac{m_e}{m_H \beta \cos^2\theta} \right).$$

When $\beta \gg 1$ (see Foote & Kulsrud 1979),

$$\Gamma_L = \begin{cases} 2\omega^2/\Omega_i, & k < \Omega_i/\beta V_A, \\ 2\Omega_i/\beta, & k > \Omega_i/\beta V_A, \end{cases} \tag{A5}$$

where Ω_i is the ion gyrofrequency.

A4. ION VISCOSITY

In a strong magnetic field ($\Omega_i \tau_i \gg 1$), the transport of transverse momentum is prohibited by the magnetic field (along $\hat{z}$). Thus, the transverse viscosity $\eta_\perp$ is much smaller than the longitudinal viscosity η_0, $\eta_\perp \sim \eta_0/(\Omega_i \tau_i)^2$. Following Braginskii (1965), we find that the damping rate is (see Yan & Lazarian 2004)

$$\Gamma_{\text{ion}} = \begin{cases} k_\perp^2 \eta_0/6\rho_i, & \beta \ll 1, \\ k^2 \eta_0 (1 - 3\cos^2\theta)^2/6\rho_i, & \beta \gg 1. \end{cases} \tag{A6}$$

For more discussion, see Yan & Lazarian (2004).

APPENDIX B

FOKKER-PLANCK COEFFICIENTS

In QLT, the effect of MHD waves is studied by calculating the first-order corrections to the particle orbit in the uniform magnetic field and ensemble-averaging over the statistical properties of the MHD waves (Jokipii 1966; Schlickeiser & Miller 1998). Obtained by applying the QLT to the collisionless Boltzmann-Vlasov equation, the Fokker-Planck equation is generally used to describe the evolvement of the gyrophase-averaged particle distribution,

$$\frac{\partial f}{\partial t} = \frac{\partial}{\partial \mu} \left(D_{\mu\mu} \frac{\partial f}{\partial \mu} + D_{\mu p} \frac{\partial f}{\partial p} \right) + \frac{1}{p^2} \frac{\partial}{\partial p} \left[p^2 \left(D_{\mu p} \frac{\partial f}{\partial \mu} + D_{pp} \frac{\partial f}{\partial p} \right) \right],$$

---

[16] We corrected an error in the corresponding expression.

where p is the particle momentum. The Fokker-Planck coefficients $D_{\mu\mu}$, $D_{\mu p}$, and D_{pp} are the fundamental physical parameters for measuring the stochastic interactions,

$$
\begin{pmatrix} D_{\mu\mu} \\ D_{\mu p} \\ D_{pp} \end{pmatrix} = \frac{\pi\Omega^2(1-\mu^2)}{2} \int_{k_{\min}}^{k_{\max}} dk^3 \frac{\tau_k^{-1}}{\tau_k^{-2} + (\omega - k_\parallel v\mu - \Omega)^2} \begin{bmatrix} \left(1+\frac{\mu V_{\mathrm{ph}}}{v\zeta}\right)^2 \\ \left(1+\frac{\mu V_{\mathrm{ph}}}{v\zeta}\right)mV_{\mathrm{A}} \\ m^2 V_{\mathrm{A}}^2 \end{bmatrix}
$$

$$
\times \left(\left[J_2^2\left(\frac{k_\perp v_\perp}{\Omega}\right) + J_0^2\left(\frac{k_\perp v_\perp}{\Omega}\right) \right] \begin{bmatrix} M_{\mathcal{RR}}(\boldsymbol{k}) + M_{\mathcal{LL}}(\boldsymbol{k}) \\ -C_{\mathcal{RR}}(\boldsymbol{k}) - C_{\mathcal{LL}}(\boldsymbol{k}) \\ K_{\mathcal{RR}}(\boldsymbol{k}) + K_{\mathcal{LL}}(\boldsymbol{k}) \end{bmatrix} - 2J_2\left(\frac{k_\perp v_\perp}{\Omega}\right)J_0\left(\frac{k_\perp v_\perp}{\Omega}\right) \left\{ e^{i2\phi} \begin{bmatrix} M_{\mathcal{RL}}(\boldsymbol{k}) \\ -C_{\mathcal{RL}}(\boldsymbol{k}) \\ K_{\mathcal{RL}}(\boldsymbol{k}) \end{bmatrix} + e^{-i2\phi} \begin{bmatrix} M_{\mathcal{LR}}(\boldsymbol{k}) \\ -C_{\mathcal{LR}}(\boldsymbol{k}) \\ K_{\mathcal{LR}}(\boldsymbol{k}) \end{bmatrix} \right\} \right),
$$

$$(B1)$$

where $|\boldsymbol{k}_{\min}| = k_{\min} = L^{-1}$, $|\boldsymbol{k}_{\max}| = k_{\max}$ corresponds to the dissipation scale, $\mathcal{L}$ and $\mathcal{R}$ refer to left- and right-circularly polarized modes, and $\phi = \tan^{-1} k_x/k_y$.

The correlation tensors are defined as

$$
\left\langle B_\alpha(\boldsymbol{k},\ t)B_\beta^*(\boldsymbol{k}',\ t+\tau) \right\rangle / B_0^2 = \delta(\boldsymbol{k}-\boldsymbol{k}')M_{\alpha\beta}(\boldsymbol{k})e^{-\tau/\tau_k}, \qquad \left\langle v_\alpha(\boldsymbol{k},\ t)B_\beta^*(\boldsymbol{k}',\ t+\tau) \right\rangle / V_{\mathrm{A}}B_0 = \delta(\boldsymbol{k}-\boldsymbol{k}')C_{\alpha\beta}(\boldsymbol{k})e^{-\tau/\tau_k},
$$

$$
\left\langle v_\alpha(\boldsymbol{k},\ t)v_\beta^*(\boldsymbol{k}',\ t+\tau) \right\rangle / V_{\mathrm{A}}^2 = \delta(\boldsymbol{k}-\boldsymbol{k}')K_{\alpha\beta}(\boldsymbol{k})e^{-\tau/\tau_k}, \tag{B2}
$$

where $B_{\alpha,\beta}$ and $v_{\alpha,\beta}$ are, respectively, the magnetic and velocity perturbations associated with the turbulence and τ_k is the nonlinear decorrelation time and essentially the cascading time of the turbulence. For the balanced cascade that we consider (see the discussion of our imbalanced cascade in CLV02), i.e., for equal intensity of forward and backward waves, $C_{ij}(\boldsymbol{k}) = 0$.

The magnetic correlation tensor for Alfvénic turbulence is (CLV02)

$$
\begin{bmatrix} M_{ij}(\boldsymbol{k}) \\ K_{ij}(\boldsymbol{k}) \end{bmatrix} = \frac{L^{-1/3}}{12\pi} I_{ij} k_\perp^{-10/3} \exp\left(\frac{-L^{1/3}|k_\parallel|}{k_\perp^{2/3}}\right), \qquad \tau_k = \left(\frac{L}{V_{\mathrm{A}}}\right)(k_\perp L)^{-2/3} \sim k_\parallel V_{\mathrm{A}}, \tag{B3}
$$

where $I_{ij} = \{\delta_{ij} - k_i k_j/k^2\}$ is a two-dimensional tensor in the x-y plane that is perpendicular to the magnetic field, L is the injection scale, and V is the velocity at the injection scale. Slow modes are passive and similar to Alfvén modes. The normalization constant is obtained by assuming equipartition $\epsilon_k = \int dk^3 \sum_{i=1}^3 M_{ii}B_0^2/8\pi \sim B_0^2/8\pi$. The normalizations for the tensors below are obtained in the same way.

According to CL02, fast modes are isotropic and have a one-dimensional energy spectrum $E(k) \propto k^{-3/2}$. In a low-β medium, the corresponding correlation is (YL03)

$$
\begin{bmatrix} M_{ij}(\boldsymbol{k}) \\ K_{ij}(\boldsymbol{k}) \end{bmatrix} = \frac{L^{-1/2}}{8\pi} H_{ij} k^{-7/2} \begin{bmatrix} \cos^2\theta \\ 1 \end{bmatrix}, \qquad \tau_k = \left(\frac{k}{L}\right)^{-1/2} \frac{V_{\mathrm{A}}}{V^2}, \tag{B4}
$$

where θ is the angle between $\boldsymbol{k}$ and $\boldsymbol{B}$ and $H_{ij} = k_i k_j/k_\perp^2$ is also a two-dimensional tensor in the x-y plane. The factor $\cos^2\theta$ represents the projection, as the magnetic perturbation is perpendicular to $\boldsymbol{k}$. This tensor is different from that in Schlickeiser & Miller (1998). For isotropic turbulence, a tensor of the form $\propto E_k(\delta_{ij} - k_i k_j/k^2)$ was obtained to satisfy the divergence-free condition $\boldsymbol{k}\cdot\delta\boldsymbol{B} = 0$ (see Schlickeiser 2002). Nevertheless, the fact that $\delta\boldsymbol{B}$ in fast modes is in the $\boldsymbol{k}$-$\boldsymbol{B}$ plane places another constraint on the tensor, so that the term δ_{ij} does not exist.

In a high-β medium, fast modes in this regime are essentially sound waves compressing the magnetic field (GS95; Lithwick & Goldreich 2001; CL03). The compression of the magnetic field depends on the plasma β. The corresponding (x, y) components of the tensors are

$$
\begin{bmatrix} M_{ij}(\boldsymbol{k}) \\ K_{ij}(\boldsymbol{k}) \end{bmatrix} = \frac{L^{-1/2}}{2\pi} \sin^2\theta H_{ij} k^{-7/2} \begin{bmatrix} \cos^2\theta/\beta \\ 1 \end{bmatrix}, \qquad \tau_k = (k k_{\min})^{-1/2} \frac{C_s}{V^2}, \tag{B5}
$$

where C_s is the sound speed. The velocity perturbations in a high-β medium are longitudinal, i.e., along $\boldsymbol{k}$; thus, we have the factor $\sin^2\theta$ and also a factor $V_{\mathrm{A}}^2/C_s^2 = 2/\beta$ from the magnetic frozen condition $\omega\delta\boldsymbol{B} \sim \boldsymbol{k}\times(\boldsymbol{v}_k\times\boldsymbol{B})$. We use these statistics to calculate grain acceleration arising from MHD turbulence.

The spherical components of the correlation tensors are obtained below. For Alfvén modes, their tensors are proportional to

$$
I_{ij} = \begin{pmatrix} \sin^2\phi & -\cos\phi\sin\phi \\ -\cos\phi\sin\phi & \cos^2\phi \end{pmatrix}. \tag{B6}
$$

Thus, we get

$$I_{\mathcal{RR}} = I_{\mathcal{LL}} = \frac{(I_x - iI_y)}{\sqrt{2}} \frac{(I_x^* + iI_y^*)}{\sqrt{2}} = \frac{1}{2}\left(I_{xx} + I_{yy}\right) = \frac{1}{2},$$

$$e^{i2\phi}I_{\mathcal{RL}} + e^{-i2\phi}I_{\mathcal{LR}} = \frac{(I_x - iI_y)^2}{2}e^{i2\phi} + \frac{(I_x + iI_y)^2}{2}e^{-i2\phi} = \left(I_{xx} - I_{yy}\right)\cos 2\phi + \left(I_{xy} + I_{yx}\right)\sin 2\phi = -1.$$

For fast modes, their tensors have the component

$$H_{ij} = Ak^{-3.5}\begin{pmatrix} \cos^2\phi & \cos\phi\sin\phi \\ \cos\phi\sin\phi & \sin^2\phi \end{pmatrix}. \tag{B7}$$

Thus, we have

$$H_{\mathcal{RR}} = H_{\mathcal{LL}} = \frac{1}{2}\left(H_{xx} + H_{yy}\right) = \frac{1}{2},$$

$$e^{i2\phi}H_{\mathcal{RL}} + e^{-i2\phi}H_{\mathcal{LR}} = \left(H_{xx} - H_{yy}\right)\cos 2\phi + \left(H_{xy} + H_{yx}\right)\sin 2\phi = 1.$$

APPENDIX C

DRAG DUE TO THE DIPOLE MOMENT OF GRAIN

Plasma drag due to rotational motion for stationary grains has been considered before (Anderson & Watson 1993; Draine & Lazarian 1998, hereafter DL98). Similarly, for a grain with electric dipole moment μ, there also exist forces between the grain and nearby ions. Consider the effects in the comoving frame of the grain. In this frame ions move at speed v with impact parameter b. To simplify the problem, we define a stopping cross section $\sigma_s = \pi b_0^2$, where b_0 is defined by $Z_i e\mu/b_0^2 = m_i v^2$. For impact parameters $b < \max(a, b_0)$, the interaction is strong. We assume

$$a < b_0 = \left(\frac{Z_i e\mu}{m_i v^2}\right)^{1/2} = (5.4 \times 10^{-7}\ \text{cm})Z_i^{1/2}\mu_1\left(\frac{m_{\text{H}}}{m_i}\right)^{1/2}\frac{1\ \text{km s}^{-1}}{v}, \tag{C1}$$

where $\mu_1 \equiv \mu/10$ D.[17] If we assume the ions to be scattered isotropically, then the drag force due to strong scattering events is

$$F_s \approx n_i Z_i e\mu\frac{4\sqrt{\pi}}{3}\frac{v_{\text{gr}}}{\max\left[v_m, (4/3\sqrt{\pi})v_{\text{gr}}\right]}, \tag{C2}$$

where $v_m = (2kT/m)^{1/2}$ is the most probable speed of ions at temperature T. For ions with impact parameter greater than b_0, we assume their trajectories are barely changed during the collisions with the grain. Define the direction of v as the polar axis $\hat{e}_z$, let the pericenter be at $(b, 0, 0)$, and let t be the time from the pericenter. The force on the ion from the dipole moment is

$$F_{\text{di}} = \frac{Z_i e}{(b^2 + v^2 t^2)^{2.5}}\left[\hat{e}_x\mu_x(2b^2 + 3vtb - v^2 t^2) + \hat{e}_z\mu_z(2v^2 t^2 + 3vtb - b^2) - \hat{e}_y\mu_y(b^2 + v^2 t^2)\right]. \tag{C3}$$

Integrated over time from $-\infty$ to ∞, this expression yields the total momentum delivered to the grain:

$$\triangle p = \frac{2Z_i e}{b^2 v}\left(-\hat{e}_x\mu_x + \hat{e}_y\mu_y\right). \tag{C4}$$

Since p increases in a random-walk fashion, the impulses of individual collisions should be added in quadrature. If we now average over random orientations of μ and then integrate over the impact parameters and thermal distribution of ion velocities, we find

$$\frac{dp^2}{dt} = n_i\int_0^\infty dv\, 4\pi v^2 f_i(v)v\int_{b_0}^{b_2} 2\pi b\, db\, \frac{2}{3}\left(\frac{2\mu Z_i e}{b^2 v}\right)^2 = \frac{16\sqrt{\pi}}{3}n_i Z_i e\mu m_i v_m, \tag{C5}$$

where for the upper cutoff we take the Debye length $b_2 = (kT/4\pi n_e e^2)^{1/2} \gg b_0$. Using the fluctuation dissipation theorem, we then can get the damping force for subsonic grains,

$$F = F_s + \frac{v_{\text{gr}}}{6kT}\frac{dp^2}{dt} = \frac{28\sqrt{\pi}}{9}n_i Z_i e\mu\frac{v_{\text{gr}}}{v_m}. \tag{C6}$$

---

[17] In DL98 it was estimated that $\mu_1 \approx 0.93(a/10^{-7}\ \text{cm})^{3/2}$.

If the grains become supersonic, the fluctuation dissipation theorem is no longer applicable. Since the interaction is elastic, the loss of the momentum in the direction parallel to the direction of motion can be obtained by assuming energy conservation: $p_z^2 + p_\perp^2 = $ const. The dipole interaction is weak, so that $\triangle p/p \ll 1$ during one encounter. Thus, we can estimate the momentum loss in the z-direction as $\Delta p_z = \triangle p_\perp^2/2p$, where $\Delta p_\perp$ is given by equation (C4). Then, integrating over the impact parameter, we get the damping force

$$F = \pi n_i Z_i e\mu + \frac{n_i}{m_i} \int_{b_0}^{b_2} 2\pi b \, db \, \frac{4}{3} \left(\frac{Z_i e\mu}{b^2}\right)^2 \frac{1}{v_{\text{gr}}^2} = \frac{7\pi}{3} n_i Z_i e\mu. \tag{C7}$$

To determine the importance of this force, we compare it with other drag forces. Using the dipole moment estimated by DL98, we find that dipole drag is smaller than collisional drag. However, for very small neutral grains with a dipole moment in ionized gas, dipole plasma drag may play a more important role.

We note that the estimate by DL98 of rotational excitation by plasma drag acting on the grain dipole moment overestimated the transfer of angular momentum by using the weak-interaction approximation for all trajectories with $b > a$. Assuming random scattering, the mean square angular momentum transfer from strong scattering events is $\sim 2(m_i vb)^2$, and thus, the contribution of impact parameters $a < b < b_0$ to dL^2/dt is

$$\frac{dL^2}{dt} \approx n_i \int_0^\infty dv \, 4\pi v^2 f_i(v) v \int_a^{b_0} 2\pi b \, db \, 2(mvb)^2 = 4\pi^2 n_i m^2 \int_0^\infty dv \, v^5 f_i(v)(b_0^4 - a^4)$$

$$= 2\sqrt{\pi} n_i \frac{Z_i^2 e^2 \mu^2}{v_m} \left(1 - \frac{2m^2 v_m^4 a^4}{Z^2 e^2 \mu^2}\right) \approx 5.71 \times 10^{-4} \hbar^2 \text{ s}^{-1} \left(\frac{n_i}{1 \text{ cm}^{-3}}\right) \left(\frac{m_i}{m_{\text{H}}}\right)^{1/2} T_2^{-1/2} Z_i^2 \mu_1^2, \tag{C8}$$

where $T_2 \equiv T/100$ K and $a_{-7} \equiv a/10^{-7}$ cm. For comparison, for impact parameters $a < b < b_0$ DL98 found

$$\frac{dL^2}{dt} = \frac{32\sqrt{\pi}}{3} n_i \frac{Z_i^2 e^2 \mu^2}{v_m} \ln\left(\frac{b_0}{a}\right) = 3.05 \times 10^{-3} \hbar^2 \text{ s}^{-1} \left(\frac{n_i}{1 \text{ cm}^{-3}}\right) \left(\frac{m_i}{m_{\text{H}}}\right)^{1/2} T_2^{-1/2} Z_i^2 \mu_1^2 \ln\left(\frac{4.07}{a_{-7}^{1/4} T_2^{1/2}}\right). \tag{C9}$$

This part of the contribution is comparable to the total if $a_{-7} \lesssim 1$ and $T_2 \lesssim 1$ or if the angle between the dipole moment and the rotation velocity is close to $90°$ (see eq. [B35] in DL98). For instance, at $T = 100$ K, for grains with $a_{-7} = 0.5$, the part given by equation (C9) is $\sim 35\%$ of the total for $\cos^2\Psi = \frac{1}{3}$. In such cases, the correction owing to the strong scattering as given in equation (C8) should be taken into account.

APPENDIX D

ANGLE BETWEEN $\boldsymbol{B}$ AND $\boldsymbol{v}$

A fundamental question arises from the fact that in MHD turbulence wavevectors are not aligned along magnetic field lines, as is the case for pure Alfvén waves. We need to analyze the relative position of three vectors: the magnetic field vector $\boldsymbol{B}$, the wavevector $\boldsymbol{k}$, and the displacement velocity vector $\boldsymbol{v}$. In what follows we study how the angle γ between $\boldsymbol{v}$ and $\boldsymbol{B}$ changes with the plasma β.

It is shown in Alfvén & Fälthmmar (1963) that the angle Ψ between $\boldsymbol{v}$ and $\boldsymbol{k}$ can be expressed as

$$\tan \Psi = \frac{\sin\theta \cos\theta}{\cos^2\theta - v_p^2/V_{\text{A}}^2}, \tag{D1}$$

where θ is the angle between $\boldsymbol{k}$ and $\boldsymbol{B}$ and the phase velocity v_p is related to the Alfvénic velocity V_{A} and the sound velocity C_s through the dispersion relation

$$v_p^4 - \left(V_{\text{A}}^2 + C_s^2\right) v_p^2 + C_s^2 V_{\text{A}}^2 \cos^2\theta = 0. \tag{D2}$$

Solving this equation for $\epsilon = v_f^2/v_{\text{A}}^2$,

$$\epsilon(\beta) = \frac{1}{2} \left[1 + \frac{\beta}{2} \pm \sqrt{\left(1 - \frac{\beta}{2}\right)^2 + 2\beta \sin^2\theta}\right], \tag{D3}$$

where the plus sign gives the result for the fast mode and the minus sign represents the slow mode. Thus, the angle γ can be calculated as

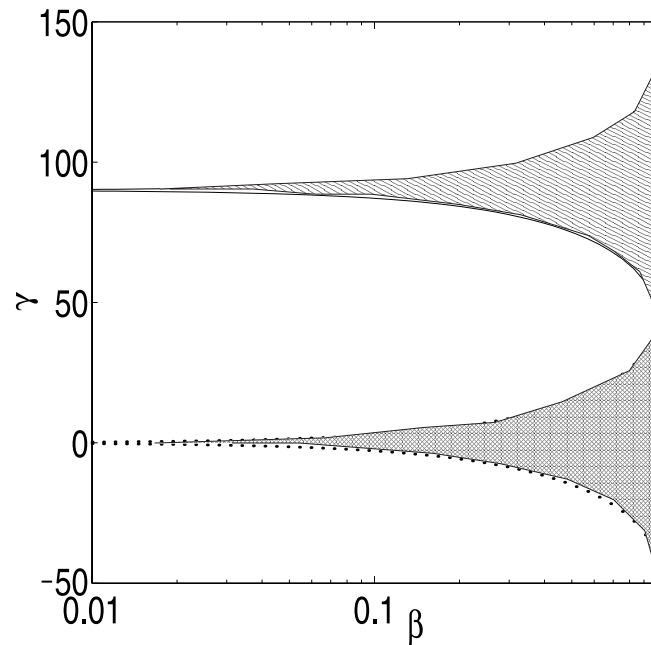$$\gamma = \theta - \arctan \frac{\sin\theta \cos\theta}{\cos^2\theta - \epsilon(\xi)}, \tag{D4}$$

FIG. 9.—Range of angles between **B** and **v**. The upper shaded area refers to the fast modes, and the lower shaded area, the slow modes. The ranges are produced by the angle between **k** and **B** changing from 0 to π.

and the corresponding plot is shown in Figure 9. It is evident that for a low-β plasma the velocity v of the fast mode is directed nearly perpendicular to **B** whatever the direction of **k**, while the velocity of the slow mode is nearly parallel to the magnetic field. Therefore, the parallel motions we get from the slow mode are essentially correct, while the perpendicular motions are also influenced by the fast mode. A more general discussion of this issue is given in CLV02.

REFERENCES

Alfvén, H., & Fälthmmar, C. G. 1963, Cosmical Electrodynamics (Oxford: Clarendon)
Anderson, N., & Watson, W. D. 1993, A&A, 270, 477
Armstrong, J. W., Rickett, B. J., & Spangler, S. R. 1995, ApJ, 443, 209
Arons, J., & Max, C. E. 1975, ApJ, 196, L77
Biermann, L., & Harwit, M. 1980, ApJ, 241, L105
Black, J. H., & van Dishoeck, E. F. 1991, ApJ, 369, L9
Blum, J. 2000, Space Sci. Rev., 92, 265
Boldyrev, S., Nordlund, Å., & Padoan, P. 2002, ApJ, 573, 678
Braginskii, S. I. 1965, Rev. Plasma Phys., 1, 205
Cho, J., & Lazarian, A. 2002, Phys. Rev. Lett., 88, 245001 (CL02)
———. 2003a, Rev. Mex. AA Ser. Conf., 15, 293 (CL03)
———. 2003b, MNRAS, 345, 325
———. 2004, in Acoustic Emission and Scattering by Turbulent Flows, ed. M. Rast (New York: Springer), in press (astro-ph/0301462)
Cho, J., Lazarian, A., Honein, A., Knaepen, B., Kassinos, S., & Moin, P. 2003, ApJ, 589, L77
Cho, J., Lazarian, A., & Vishniac, E. T. 2002a, in Turbulence and Magnetic Fields in Astrophysics, ed. T. Passot & E. Falgorone (New York: Springer), 56
———. 2002b, ApJ, 564, 291 (CLV02)
———. 2002c, ApJ, 566, L49
Cho, J., & Vishniac, E. T. 2000, ApJ, 539, 273
Chokshi, A., Tielens, A. G. G. A., & Hollenbach, D. 1993, ApJ, 407, 806
Ciolek, G. E., & Mouschovias, T. C. 1996, ApJ, 468, 749
Crutcher, R. M. 1999, ApJ, 520, 706
de Oliveira–Costa, A., et al. 2002, ApJ, 567, 363
Dominik, C., & Tielens, A. G. G. A. 1997, ApJ, 480, 647
Draine, B. T. 1985, in Protostars and Planets II, ed. D. C. Black & M. S. Matthews (Tucson: Univ. Arizona Press), 621
Draine, B. T., & Lazarian, A. 1998, ApJ, 508, 157 (DL98)
Draine, B. T., Roberge, W. G., & Dalgarno, A. 1983, ApJ, 264, 485
Draine, B. T., & Salpeter, E. E. 1979, ApJ, 231, 77
Ellison, D. C., Drury, L. O'C., & Meyer, J.-P. 1997, ApJ, 487, 197
Elmegreen, B. G., & Fiebig, D. 1993, A&A, 270, 397
Epstein, R. I. 1980, MNRAS, 193, 723
Foote, E. A., & Kulsrud, R. M. 1979, ApJ, 233, 302
Ginzburg, V. L. 1961, Propagation of Electromagnetic Waves in Plasma (New York: Gordon & Breach)

Gold, T. 1952, MNRAS, 112, 215
Goldreich, P., & Sridhar, S. 1995, ApJ, 438, 763 (GS95)
Greenberg, J. M., & Yencha, A. J. 1973, in IAU Symp. 52, Interstellar Dust and Related Topics, ed. J. M. Greenberg & H. C. van de Hulst (Dordrecht: Reidel), 369
Higdon, J. C. 1984, ApJ, 285, 109
Hildebrand, R. H., Davidson, J. A., Dotson, J. L., Dowell, C. D., Novak, G., & Vaillancourt, J. E. 2000, PASP, 112, 1215
Jokipii, J. R. 1966, ApJ, 146, 480
Jones, A. P., Tielens, A. G. G. M., & Hollenbach, D. J. 1996, ApJ, 469, 740
Kim, S. H., Martin, P. G., & Hendry, P. D. 1994, ApJ, 422, 164
Kulsrud, R. M., & Pearce, W. P. 1969, ApJ, 156, 445
Kusaka, T., Nakano, T., & Hayashi, C. 1970, Prog. Theor. Phys., 44, 1580
———. 1999, in Plasma Turbulence and Energetic Particles in Astrophysics, ed. M. Ostrowski & R. Schlickeiser (Krakow: Obs. Astron.), 28
———. 2000, in ASP Conf. Ser. 215, Cosmic Evolution and Galaxy Formation, ed. J. Franco, E. Terlevich, O. Lopez-Cruz, & I. Aretxaga (San Francisco: ASP), 69
———. 2003, J. Quant. Spectrosc. Radiat. Transfer, 79, 881
Lazarian, A., & Pogosyan, D. 2000, ApJ, 537, 720
Lazarian, A., & Vishniac, E. 1999, ApJ, 517, 700
Lazarian, A., Vishniac, E., & Cho, J. 2004, ApJ, 603, 180
Lazarian, A., & Yan, H. 2002a, ApJ, 566, L105 (LY02)
———. 2002b, Best Sci., submitted (astro-ph/0205283)
———. 2004, in ASP Conf. Ser. 309, Astrophysics of Dust, ed. A. N. Witt, G. C. Clayton, & B. T. Draine (San Francisco: ASP), 479
Lepp, S. 1992, in IAU Symp. 150, Astrochemistry of Cosmic Phenomena, ed. P. Singh (Dordrecht: Kluwer), 471
Lithwick, Y., & Goldreich, P. 2001, ApJ, 562, 279
Maron, J., & Goldreich, P. 2001, ApJ, 554, 1175
Mathis, J. S., Rumpl, W., & Nordsieck, K. H. 1977, ApJ, 217, 425
Mathis, J. S., & Whiffen, G. 1989, ApJ, 341, 808
McCall, B. J., et al. 2003, Nature, 422, 500
Melrose, D. B. 1980, Plasma Astrophysics (New York: Gordon & Breach)
Montgomery, D., & Matthaeus, W. 1981, Phys. Fluids, 24, 825
Mukherjee, P., Jones, A. W., Kneissl, R., & Lasenby, A. N. 2001, MNRAS, 320, 224
Nishi, R., Nakano, T., & Umebayashi, T. 1991, ApJ, 368, 181
Ossenkopf, V. 1993, A&A, 280, 617

Pryadko, J. M., & Petrosian, V. 1997, ApJ, 482, 774
Purcell, E. M. 1969, Physica, 41, 100
———. 1979, ApJ, 231, 404
Ruffle, D. P., Hartquist, T. W., Rawlings, J. M. C., & Williams, D. A. 1998, A&A, 334, 678
Scalo, J. M. 1987, in Interstellar Processes, ed. D. J. Hollenbach & H. A. Thronson, Jr. (Dordrecht: Reidel), 349
Schlickeiser, R. 2002, Cosmic Ray Astrophysics (Berlin: Springer)
Schlickeiser, R., & Miller, J. A. 1998, ApJ, 492, 352
Schutte, W. A., & Greenberg, J. M. 1991, A&A, 244, 190
Shebalin, J. V., Matthaeus, W. H., & Montgomery, D. 1983, J. Plasma Phys., 29, 525
Spitzer, L. 1978, Physical Processes in the Interstellar Medium (New York: Wiley)

Stanimirovic, S., & Lazarian, A. 2001, ApJ, 551, L53
Stepanov, K. N. 1958, Soviet Phys.–JETP, 34, 1292
Völk, H. J., Jones, F. C., Morfill, G. E., & Roser, S. 1980, A&A, 85, 316
Wakker, B. P., & Mathis, J. S. 2000, ApJ, 544, L107
Weidenschilling, S. J., & Ruzmaikina, T. V. 1994, ApJ, 430, 713
Weingartner, J. C., & Draine, B. T. 2001a, ApJ, 553, 581
———. 2001b, ApJS, 134, 263
———. 2001c, ApJ, 563, 842
Welty, D. E., Hobbs, L. M., Lauroesch, J. T., Morton, D. C., Spitzer, L., & York, D. G. 1999, ApJS, 124, 465
Yan, H., & Lazarian, A. 2002, Phys. Rev. Lett., 89, 281102 (YL02)
———. 2003, ApJ, 592, L33 (YL03)
———. 2004, ApJ, 614, 757
Zank, G. P., & Matthaeus, W. H. 1992, J. Plasma Phys., 48, 85